CORA Cork Open Research Archive
Cartlann Taighde Oscailte Chorcaí

Title	Non-linear dynamics and critical transitions in neonatal brain
Authors	Papanikolaou, Georgios
Publication date	2024
Original Citation	Papanikolaou, G. 2024. Non-linear dynamics and critical transitions in neonatal brain. MSc Thesis, University College Cork.
Type of publication	Masters thesis (Research)
Rights	© 2024, Georgios Papanikolaou. - https://creativecommons.org/publicdomain/zero/1.0/
Download date	2026-11-15 14:01:43
Item downloaded from	https://hdl.handle.net/10468/17925



UCC
University College Cork, Ireland
Coláiste na hOllscoile Corcaigh

Non-linear dynamics and critical transitions in neonatal brain

Georgios Papanikolaou, MSc

https://orcid.org/0000-0003-2864-0440

Thesis submitted for the degree of

Master of Science



University College Cork, Ireland

School of Mathematical Sciences

Supervisor: Prof. Sebastian Wieczorek

Co-Supervisor: Dr. Andreas Amann

Head of School: Dr. Kevin Hayes

December 2024

Contents

1 Introduction **5**

2 The INFANT dataset **9**

2.1 Data acquisition and labelling 10

2.2 Processing of raw EEG data 12

2.3 Seizure Selection 16

3 Methodology **19**

3.1 Theoretical background 19

3.1.1 Early Warning Signal in Critical transitions 20

3.1.2 Early warning signals in epileptic seizures 26

3.2 Feature Estimation Methods 28

3.2.1 Gaussian weighted variance 29

3.2.2 Exponential weighted variance 30

3.2.3 Rolling autocorrelation 31

3.2.4 Measure of statistical significance of binary indicators . . . 37

3.2.5 Finding 'optimal' feature estimation method parameters . 38

4 Results **43**

4.1 Early warning signals on HIE seizure onsets 43

4.1.1 Examples of seizure onsets using the 'optimal' parameters 46

4.2 Analysis and comparison of the results between the neonates . . . 49

5 Discussion **51**

6 Appendix A **55**

6.1 Proofs . . . 55

6.1.1 Reparametrisation of h . . . 55

6.2 Code for EEG . . . 57

6.2.1 Preprocessing Filter . . . 57

6.2.2 Calculate the increase or decrease of variance and autocorrelation prior to a seizure event . . . 59

6.3 Code for Feature Estimation Methods . . . 61

6.3.1 Gaussian Weighted Variance . . . 61

6.3.2 Exponential Weighted Variance . . . 63

6.3.3 Autocorrelation . . . 63

6.4 Code for Harvested Population system . . . 67

6.4.1 Bifurcation Diagram . . . 67

6.4.2 Numerical calculations of the Harvested population and the linearized Harvested population system . . . 68

Declaration

This is to certify that the work I am submitting is my own and has not been submitted for another degree, either at University College Cork or elsewhere. All external references and sources are clearly acknowledged and identified within the contents. I have read and understood the regulations of University College Cork concerning plagiarism and intellectual property.

Abstract

Neonatal seizure detection methods have improved the quality of life for new born babies. However, most models suffer from an increased amount of false positive detections that restricts them from being used live in an Neonatal Intensive Care Unit. If the dynamical mechanisms responsible for transitions to seizure states can be understood, it may be possible to enhance the methods used for the detection of seizure events. One potential candidate to describe the events that trigger a seizure is a 'critical transition'. Classical early warning signals, such as increased variance and autocorrelation, have proven to be robust measures for the detection and prediction of critical transitions in many different scenarios. In this study, we examine whether these classical early warning signals are present in EEG recordings of neonatal seizures.

Chapter 1

Introduction

According to World Health Organization, epilepsy is a brain condition that effects 50 million people world wide. Epileptic seizures are caused by abnormal brain activity, however, there is no universally accepted theory on the mechanisms responsible for triggering such seizures. Even though we don't know the underline mechanics, there are specific brain conditions that are known to enhance the propensity for epileptic seizures, like Hypoxic Ischemic Encephalopathy, traumatic brain injury and brain tumours.

In this dissertation, we focus on a condition named Hypoxic-Ischemic Encephalopathy (HIE). It is a type of brain damage that is caused by a lack of oxygen to the brain before or shortly after birth. HIE is one of the most serious complications in full term neonates [9]. It effects approximately 0.2% of neonates in developed countries. Around $20-50\%$ of infants with HIE die in infancy, while $25-60\%$ of the surviving infants have long-term neurological disorders [18].

While there is no clear proof, neurophysiologist believe that the intensity of seizures in the early stages of the brain development affect the evolution of long-term neurological disorders. To fight the development of the long-term symptoms, neurophysiologists use targeted medications and therapeutic hypothermia

to reduce the damage caused by the seizure [13].

In recent years, there has been an enormous improvement in our understanding of seizure dynamics thanks to advances in electroencephalogram (EEG) technologies that are used to record neural activity patterns in the brain of animals [11] and humans [6]. However, in comparison with the human adult brain, the dynamical features of seizures in the neonatal brain (the brain of new born babies), has proven to be more difficult to decipher [14]. For instance, accurately annotating neonatal EEG recordings of seizures is particularly challenging due to the absence of physical symptoms related to seizures as only $\approx 4.5\%$ of seizure prone neonates exhibit spasms [5].

As it is impractical to have one neurophysiologist over each neonate at all time to oversee the EEG recordings and treat the neonates based on their observations, experts usually record and analyse the data once every few hours. Even with this approach, analysing hours of data for each neonate is a time consuming approach. Moreover, due to the complexity of the seizures in the neonates brain, it is a common phenomenon for the seizure annotations of various neurophysiologists not to match with each other. This happens because experts may miss a seizure event due to the high amount of data they have to process or because a seizure event is not "strong" enough to be clearly observed. Additionally, different neurophysiologists may mark the start and end time of the same seizure event at different time points. When this happens, neurophysiologist have to spend more time to resolve these inconsistencies by conferring with each other.

To combat the above issues and relieve some of the pressures placed on neonatal intensive care units, in [21], Temko *et al.* presented a machine learning (ML) approach for detecting the occurrence of seizures in neonatal EEG recordings with a success rate of 89%. This ML model is trained on various EEG trace features in order to categorise a given EEG recording as either a seizure or non-seizure

event. The resulting ML model they developed is designed to be used both on EEG recording and "live", meaning that the model can detect the seizure while it happens with a small delay of a few seconds. While this innovation in seizure detection has enhanced the care of neonates [1], understanding mechanics that trigger a seizure event may further improve the detection of these events. In this study we explore whether the mechanics that triggers a seizure event is that of a 'critical transition'.

Critical transitions play a pivotal role in the dynamics of numerous systems in nature and describe the phenomenon whereby there is an abrupt change in the behaviour of a given system that may occur due to slowly varying changes in the system's parameters [10]. For example, critical transitions describe, the sudden extinction in population density models [16] and changes in the circulation of the Gulf stream [2]. In the case of the brain, critical transitions are thought to trigger the onset and offset of seizures [8].

In [16], Scheffer *et al.* put forward different methods for extracting early warning signals of critical transitions using measurements from a given system. It is shown here that, prior to a particular critical transition, there is a distinct increase in the variance and autocorrelation in the evolution of the system's state over time. In [12], these methods are applied to EEG recordings of epileptic human brains and show that, prior to a specific type of seizure, there is an associated change in the variance and autocorrelation in neural activity. In this study we investigate whether these methods can be extended to cater for the case of the neonatal brain.

In this dissertation, we expand the work of Scheffer et.al [16] and Milanowski and Suffczynski [12] on neonatal seizures. We work with EEG recordings of neonates with HIE from the dataset of INFANT Research Centre. We develop methods that can detect the existence of early warning signals for critical transi-

tions and check whether these early warning signals exist prior to seizures in the neonatal brain. Lastly, we draw our conclusions based on our analysis and the data we used.

This thesis is split into 5 chapters: 1) the Introduction, 2) the Infant Dataset, 3) the Methodology, 4) the Results and finally 5) the Conclusion. In Chapter 2, we delve into the acquisition and preprocessing of the INFANT dataset that we use in our study. In Chapter 3, we focus on the theoretical background and the methods used to detect early warning signals for critical transition. We provide an example showcasing these methods and we present the steps we follow to decide whether neonatal seizure exhibit early warning signals of critical transitions. Chapter 4 contains the results of our analysis. Finally, in Chapter 5 we discuss the outcome of our analysis, its limitations and future work related to our study.

Chapter 2

The INFANT dataset

In this study, we used a dataset of EEG recordings captured in the Neonatal Intensive Care Unit (NICU) of Cork University Maternity Hospital, Cork, Ireland, recorded over a 2 year period. During this period, 55 neonates were recruited with various conditions and EEGs were recorded for up to 77 hours, for each neonate. Of the 55 newborns, 17 are full-term and have been diagnosed with HIE. The severity of HIE is measured using the Sarnat score [15], a classification scale that assesses neonatal HIE through physiological symptoms such as muscle tone, respiration, alertness, etc. The 17 neonates we study have been classified with either a mild, moderate or severe Sarnat grade.

The same dataset used in this study was also used in [21] to create a model that identifies seizures in a given EEG recording. In our analysis, we focus on the pre-seizure time interval and we try to find characteristic behaviours we can detect in the EEG that can be used to identify the exact moment a seizure starts.

In this section, we describe the setup used for capturing the EEG recordings, the preprocessing of the data, and the selection of the data that we use from this dataset.

2.1 Data acquisition and labelling

A Viasys NicOne video EEG machine was used to record multi-channel EEG at a sampling rate of 256Hz using the 10–20 system of electrode placement modified for neonates as illustrated in Fig. 2.1. In Fig. 2.1, we highlight the location of the recorded EEG electrodes, $\{T3, F3, C3, O1, Cz, F4, C4, O2, T4\}$.

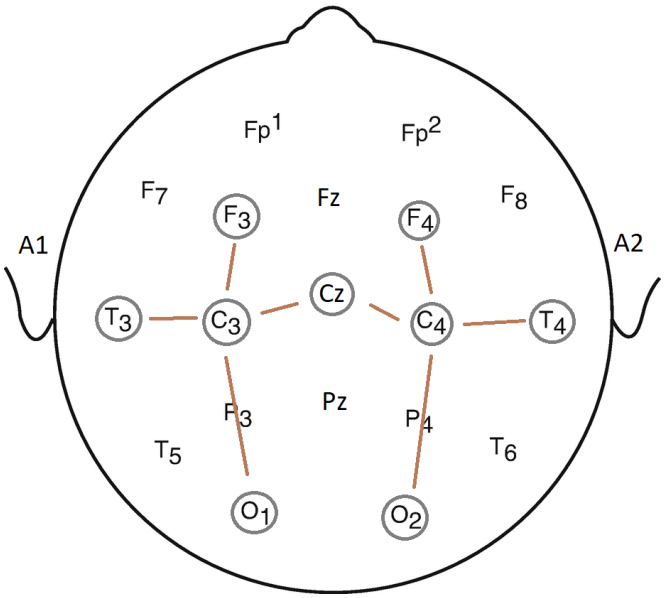


Figure 2.1: Schematic of the 10-20 system of electrode placement used to record the INFANT dataset. The circled channels are the EEG electrodes used in this paper and the orange connections between electrodes indicate the pairs of channels that construct the bipolar montage.

The EEG recordings of each neonate in the INFANT dataset range from 19 to 77 hours. The resulting data was annotated by neurophysiologists with expertise in neonatal EEG analysis following the definition of a seizure as specified in [3]. According to these criteria, an abnormal event is considered to be a seizure if it has a "sudden, repetitive, evolving, stereotyped waveform with a definite beginning, middle, and end", and has a duration of more than 10 seconds.

Seizures fall in two categories:

1. Generalized seizure: this type of seizure involve the entire brain. This means that the experts are able to detect this seizure in all EEG electrodes.

2. Focal seizure: this type of seizure involve only specific areas of the brain. This means that the experts are able to detect this seizure only in specific EEG electrodes.

If an event follows the above description of a seizure but its duration is less than 10 seconds then it is categorised as a "brief rhythmic discharge".

For future reference, we call the time that the experts have annotated as the start / end of a seizure as the onset / offset time of the seizure. Similarly, any time interval that is preceding / following the onset / offset time of a seizure is called an onset / offset time interval of the seizure, respectively. Finally, any dynamics that can be observed in the EEG recording before / after a seizure that are associated with or generated by the seizure are called onset / offset dynamics of the seizure, respectively. Such dynamics are usually waveforms close to the frequency of the seizure with lower amplitude and similar patterns. In Figure 2.2, we showcase these notions using EEG in a bipolar montage as we explain in Section 2.2. The seizure event is annotated with the red box. The onset time is at $40s$ and the offset time is at $59s$, which are the start and the end of the red box. We annotate with the orange box the possible onset dynamics and with the magenta box the possible offset dynamics. Here we observe that the waveforms in the orange and magenta boxes are similar with the waveforms during the seizure, but they are not annotated as seizures by the experts. Finally, the time intervals $[1, 40]$, $[10, 40]$ and $[20, 40]$ are examples of onset time intervals while the time intervals $[59, 65]$, $[59, 70]$ and $[59, 80]$ are examples of offset time intervals. Generally, any time interval of the form $[a, 40]$, for $a < 40$, is called

onset time intervals and any time interval of the form $[59, b]$, $b > 59$, is called an offset time interval.

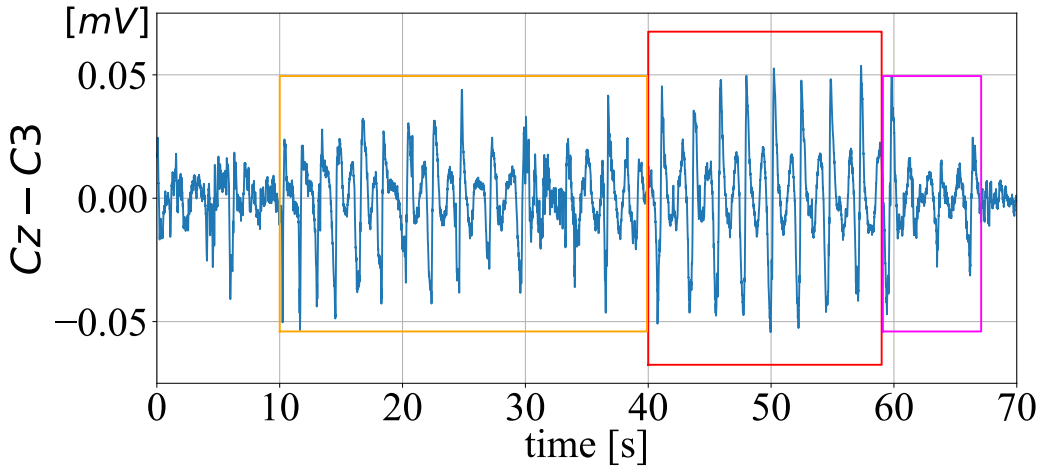


Figure 2.2: Neonatal EEG exhibiting a seizure event as annotated by experts (Red box). Orange box: Abnormal dynamics prior to the seizure event. Magenta box: Abnormal dynamics after the seizure event.

The INFANT dataset we use consists of 1278 annotated seizures. The duration of seizures ranges from 10 seconds to 40 minutes. Table 2.1 shows the number of seizures for each neonate and the corresponding mean duration of seizures for each neonate in minutes. We observe in Table 2.1 that both the number of seizures and their mean duration vary from neonate to neonate.

2.2 Processing of raw EEG data

The EEG recordings are measured and stored using a 'referential montage' where the activity of selected regions of the brain are measured as potential differences (in units of Volts) in reference to an inactive point. In order to reduce any

Table 2.1: Number of seizures, and mean of the duration of seizures.

No. Neonate	# Seizures	Mean(m)	No. Neonate	# Seizures	Mean(m)
1	17	1.5	10	201	5.0
2	3	4.2	11	41	4.5
3	209	1.8	12	43	2.45
4	84	1.6	13	150	1.6
5	63	6.5	14	60	3.4
6	4	9.5	15	21	8.2
7	46	1.1	16	121	1.5
8	99	1.5	17	19	4.6
9	17	5.9			

topological biases present in the montage, whereby the relative position of measurement channels influence one another, and model the activity of the brain in relation to its neighbouring channels, in [21] a 'bipolar montage' is constructed where the activity of selected regions of the brain is measured as potential differences between two channels. The resulting pairs of channels that are studied are $\{F4-C4, C4-O2, F3-C3, C3-O1,\ T4-C4, C4-Cz, Cz-C3, C3-T3\}$, and this setup is used in this study. In Fig. 2.1, the connecting lines between the recording channels emphasise the layout of the bipolar montage.

As an example, Fig. 2.3 displays 4 minutes of continual EEG recordings from Neonate 3 in Table 2.1. The characteristic features of neonatal seizures are difficult to decipher from the raw EEG recordings shown in Fig. 2.3. To address this issue, a band-pass filter is implemented to retain frequencies between $0.5-70\,\text{Hz}$, which is the frequency range where neonatal brain activity patterns are expected [19]. Additionally, a $50\,\text{Hz}$ notch filter (a notch filter cuts out a specific frequency from the signal) is used to suppress the utility frequency of

the power supply [4]. In Fig. 2.4, we show the resulting filter that we apply to the bipolar montage of the EEG data. The calculation of the filter is given in Appendix 6.2.1.

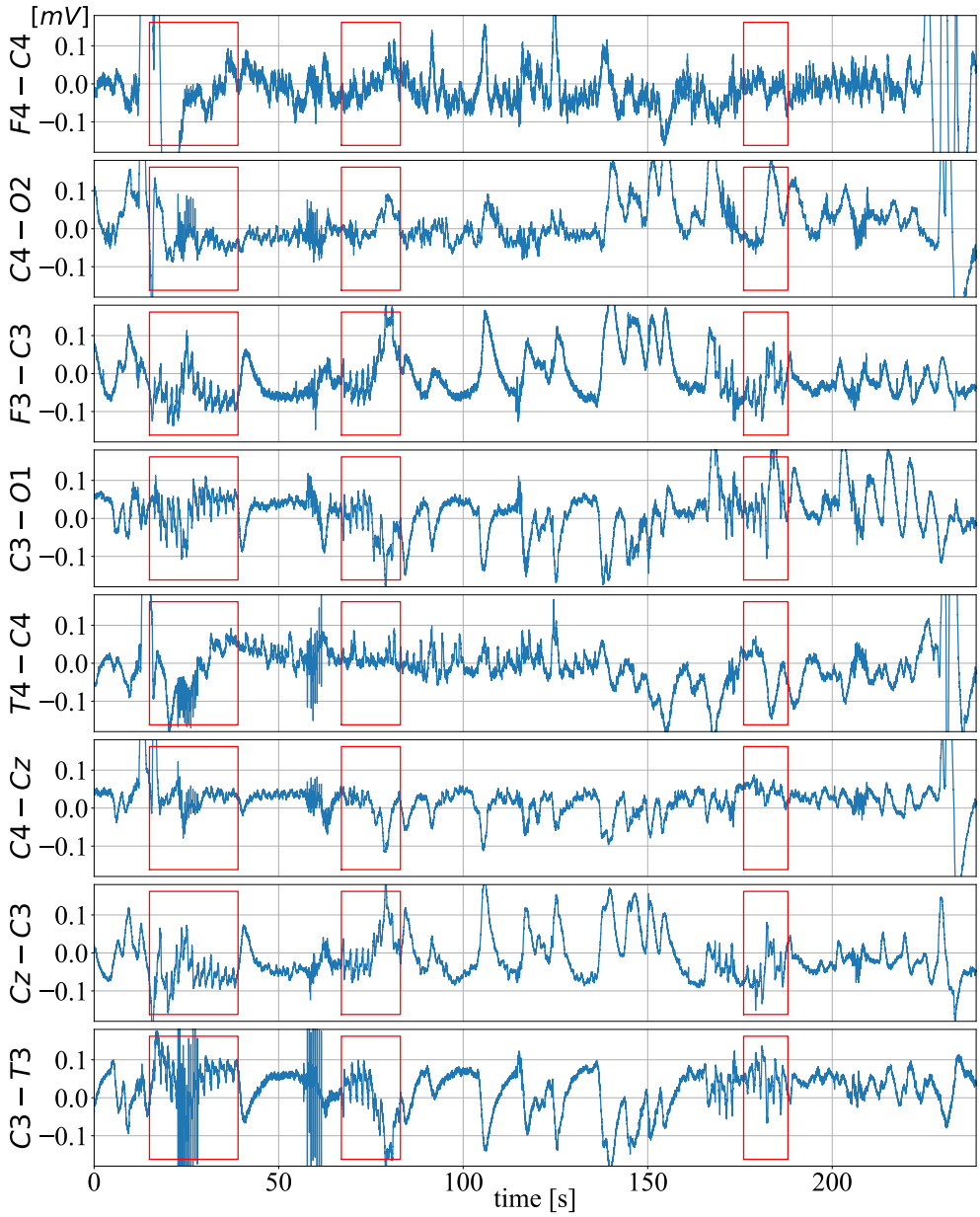


Figure 2.3: Raw bipolar montage EEG recordings of Neonate 3 over an interval of 4 minutes. Red boxes: seizure intervals as annotated by experts.

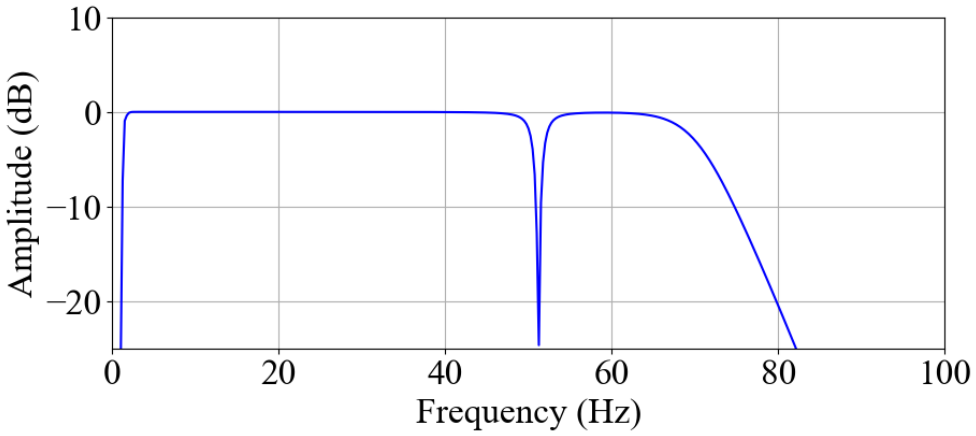


Figure 2.4: Filter response used on the EEG data. The filter is a bandpass filter at $0.5 - 70\,\text{Hz}$ and a notch filter at $50\,\text{Hz}$

The transition from a non-seizure state to a seizure state is more easily seen in Fig. 2.5 where the first seizure from Fig. 2.3 is shown here, before and after applying the above filtering process. As we see in Fig. 2.5, the filtered data are smoother and it is easier to detect changes in the EEG waveforms. The characteristic change in neural dynamics, from a small amplitude oscillation to a sudden much larger amplitude and sustained oscillation for approximately $15s$, is seen here in the $Cz - C3$ filtered EEG data. The $C4 - Cz$ panel in Fig. 2.5 does not exhibit these characteristic features to the same extent. Additionally, in the filtered data, we can more easily distinguish the onset dynamics of the seizure in the $Cz - C3$ pair during the time interval $[10 - 15]$. It is these onset dynamics that we aim to identify in the later sections.

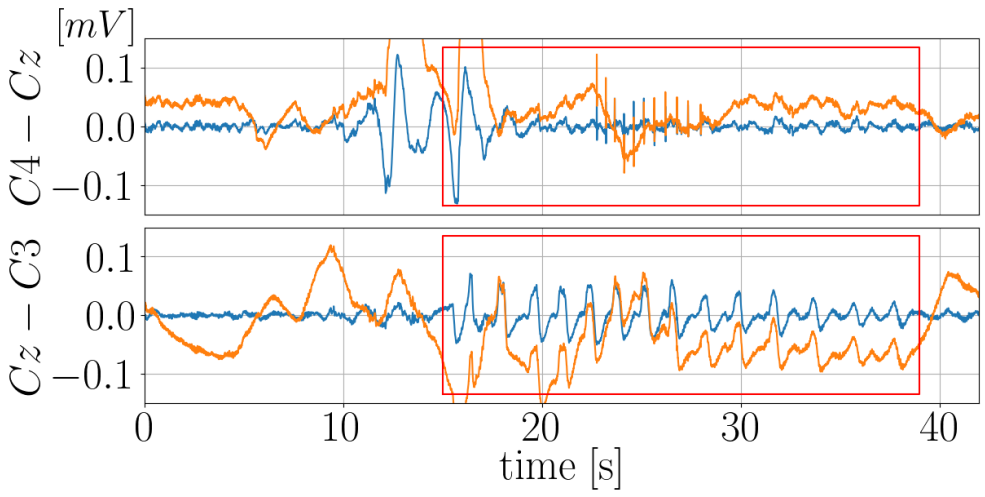


Figure 2.5: Filtered EEG recordings of the first seizure in Fig. 2.3 for the channel pairs of $C4-Cz$ and $Cz-C3$ after applying a band pass filter at $[0.5, 70]$Hz and a notch filter at 50Hz. Blue: Filtered EEG data. Orange: Unfiltered EEG data. Red boxes: seizure intervals as annotated by experts.

2.3 Seizure Selection

Before moving on to the analysis of the EEG recordings, we perform a seizure selection, meaning that we focus our study on specific seizures that we describe in this section. We perform this selection so that we have more coherent results in our analysis. This selection takes effect in Section 4, where we present the results of our analysis on the neonatal data of the INFANT dataset.

As the level of severity for each neonate's condition varies within the INFANT data set, we analyse every neonate individually. Additionally, each neonate's brain is damaged in a different region, which impacts the dynamics that are present in each pair of EEG recordings. Neurophysiologists have noted that seizures are typically more prominent and easier to detect in one or two specific bipolar pairs compared to others. For example, in Neonate 3, the bipolar pair that captures the most seizures is $Cz - C3$. If we look back in Fig. 2.5, the

seizure can be observed quite clearly in the bipolar pair $Cz - C3$, but if we look at the $C4 - Cz$ pair alone, it is not clear that a seizure is occurring at that point in time. The bipolar pair that captures the most seizures is usually the same pair where the seizures are exhibited with the clearest way. This pair is not known in advance, and is different for each neonate. Therefore, we analyse the seizure annotations for each neonate, we find, for each neonate, the pair of recording channels that is involved in the most seizure events and we concentrate our study on the EEG recordings of this pair.

After selecting the bipolar pair that we are going to study, we turn our attention to the time interval prior to seizures. Specifically, we want the onset dynamics of seizures we study to not overlap with the offset dynamics of the previous seizure. This way we can ensure that the during the time intervals we study, the onset dynamics we aim to detect are independent from the offset dynamics of the preceding seizure. For example, in Figure 2.6, looking at the inter-seizure interval at the $Cz - C3$ pair, the dynamics observed in between the two seizure events belong either to the offset dynamics of the preceding seizure, the onset dynamics of the oncoming seizure or both.

Taking this into consideration, in our experiments, we focus only on seizures with a relatively long prior inter-seizure interval and we assume the following, based on empirical knowledge of neurophysiologists:

- The duration of the onset dynamics of a seizure is less than 60 seconds.
- The offset dynamics of a seizure lasts less than 30 seconds.

Thus, we choose to study seizures whose prior inter-seizure interval is greater than 90 seconds and we select 60 second of time intervals prior to the seizure to study. These selected time intervals of 60 seconds are referred to as the 'studied intervals'.

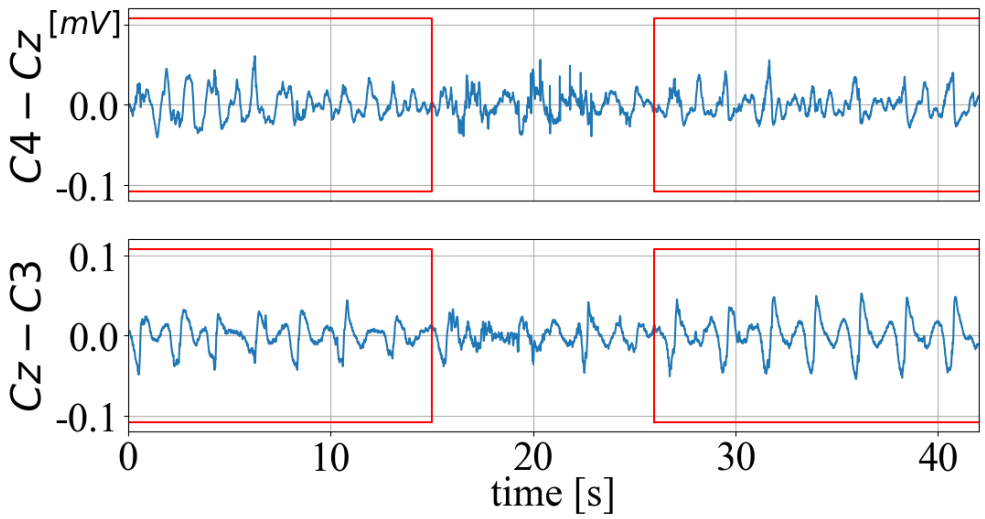


Figure 2.6: Filtered bipolar EEG recordings of Neonate 3 showcasing the offset dynamics. Red boxes: seizure intervals as annotated by experts.

For our analysis we use the neonates 3, 10 and 13 from Table 2.1. We choose these neonates for this study as they exhibit the most seizures and have a variety of Sarnat grades, meaning they have different levels of brain damage. Neonate 3 has a severe Sarnat grade and exhibits a total of 209 seizures (of which 194 are generalised seizures) during 31 hours of measurements. The $C3 - Cz$ channel is the one with the most recorded seizures and thus, out of the 209 seizures, the studied intervals consists of 151 events. Neonate 10 has a severe Sarnat grade and exhibits a total of 201 seizures (of which 170 are generalised seizures) during 68 hours of measurements. The $C4 - O2$ channel is the one with the most recorded seizures and thus, out of the 201 seizures, the studied intervals consists of 138 events. Neonate 13 has a moderate Sarnat grade and exhibits a total of 150 seizures (of which 115 are generalised seizures) during 54 hours of measurements. The $F3 - C3$ channel is the one with the most recorded seizures and thus, out of the 150 seizures, the studied intervals consists of 123 events.

Chapter 3

Methodology

In this section, we introduce the methodology used in our study. First, we briefly present the work of Scheffer et.al. [16] and Milanowski and Suffczynski [12], who describe the statistical measures we are going to use to capture the characteristic behaviour of EEG signals prior to a seizure. Then, we define the parametrised numerical methods used to estimate the statistical measures that Scheffer et.al. introduced. Afterwords, we explain how we decide the significance of the characteristic behaviour prior to a seizure we detect based on the statistical measures we estimate. And finally, we illustrate the steps used to to find the optimal parameters for estimating the statistical measures. The parameters used in the numerical methods are optimised with respect to the significance of the characteristic behaviour they detect.

3.1 Theoretical background

The purpose of this study is to investigate whether there exist any potential early warning signals prior to the onset of neonatal seizures. Early warning signals are called characteristic behaviours that are observed prior to abrupt changes in the

behaviour of a system. In our analysis, we focus on abrupt changes caused by classical bifurcations [20].

3.1.1 Early Warning Signal in Critical transitions

Scheffer et al. in [16], investigates the presence of early warning signals in 'critical transitions'. Initially, critical transitions were regarded as catastrophic events [17]. In such events, an attractor in a noise-free system either ceases to exist or transforms into a repeller. Consequently, the system's state must undergo a sudden shift, either converging towards a new attractor or diverging entirely. In recent years, the concept of critical transitions has broadened. Much like catastrophic events, critical transitions are identified as abrupt changes in the system's behaviour, resulting in a transition from one state to another [12].

According to Scheffer et.al. in [16], a system is anticipated to "critically slow down" before going through a critical transition. The notion of "critically slowing down" refers to how fast the system reacts to external or internal perturbations, such as external noise introduced by the environment of the system. In their work [16], they introduce various measures that can be used to identify upcoming critical transitions, like for example variance, autocorrelation, spatial patterns, and more. Unfortunately, many of those measures cannot be applied to our analysis, for example the detection of spacial patterns arising in dynamical systems that model space-related models, like the movement of predators in an area. From the features that Scheffer et.al. introduced, variance (var) and autocorrelation (a_corr) are the two metrics we use to measure the "critically slowing down" behaviour of the brain dynamics in the EEG recordings. In [16], the authors perform a static analysis on a "Harvested Population" system that exhibits a "saddle-node" bifurcation and showcases an increase in variance and autocorrelation prior to the system's bifurcation. We also study this system in

Sec. 3.1.1, where we study the expected change in its behaviour prior to the critical transition it exhibits and, once again, in Sec. 3.2.3, once we have introduced the methodology we use to capture the change of a system's behaviour prior to a critical transition.

Canonical Example (Part One): Static analysis of the Harvested Population system

During this example, we focus on the dynamics of the Harvested Population system to showcase the expected change in variance and autocorrelation prior to a critical transition. The harvested population system represents an ecosystem where an organism can sustain itself at the population of K 'population units' and is harvested by c. Originally, this population was thought to be the mass of the fish in a lake and the c was the amount of fishing performed. In this section, we perform a 'static analysis' (when the behaviour of the system stays the same over time) to showcase the change in the variance and autocorrelation of the system's state when the system approaches a critical transition. Next, in Sec. 3.2.3, we continue this example and perform a 'dynamical analysis' (when the behaviour of the system changes over time) using the methodology introduced in Sec. 3.2.

The 'harvested population' (HP) system, studied in [16], provides a straightforward example to study how a critical transition takes place. The dynamics of the HP system is described by the following differential equation,

$$\dot{x} = x\left(1 - \frac{x}{K}\right) - c\frac{x^2}{x^2+1} + \sqrt{D}\,\eta(t), \tag{3.1}$$

where $x(t)$ is the state of the system at time t, $f(x;c) = x\left(1-\frac{x}{K}\right) - c\frac{x^2}{x^2+1}$, K is called the carrying capacity, c is called the harvesting rate and $\eta(t)$ is the additive white noise with noise strength $D/2$. If we set $D = 0$, then we refer to

Eq. (3.1) as the the noise-free HP system. For this example (part one and two), we consider $K = 10$ and $D = 0.2$, unless stated otherwise.

To provide some insight into the HP system's dynamics, we plot the corresponding one-parameter bifurcation diagram in the (c, x)-plane for $K = 10$ and $D = 0$ in Figure 3.1. We calculate the branches of equilibria in Figure 3.1 as shown in Appendix 6.4.1.

We observe here that, for the given values of c, there are two branches of stable fixed points, denoted as $x_1(c)$ and $x_3(c)$, and two branches of unstable fixed points, denotes as $x_2(c)$ and $x_4(c)$. Two saddle-node bifurcations are also found to occur at c approximately equal to 1.8 and 2.6. These bifurcations are responsible for the critical transitions that can be brought about by changing c as the system evolves in time. Based on these findings, for our example, we call the parameter c the bifurcation parameter of the system, as it is the parameter we vary to observe these bifurcations.

Linearization

In this section, we also study the dynamics of the linearised HP system close to $x_1(c)$ [20]. This linearised HP system is determined by taking the derivative of Eq. (3.1) with respect to x and it is written as,

$$\dot{\bar{x}}(t; c) = -\lambda(c)(\bar{x}(t; c) - x_1(c)) + \sqrt{D}\,\eta(t), \tag{3.2}$$

where $\bar{x}(t; c)$ is the state of the linearised HP system and $\lambda(c)$ is calculated as the gradient of $f(x; c)$, which is one-dimensional, thus $\lambda(c) = -\frac{df}{dx}(x_1(c); c)$. Hence, $\lambda(c)$ is calculated as

$$\lambda(c) = \frac{2x_1(c)}{K} + \frac{2cx_1(c)}{(1 + x_1(c)^2)^2} - 1.$$

In Figure 3.2, we show the value of $\lambda(c)$ as the value of c gets closer to the bifurcation point. We observe that as c approaches the bifurcation point at $c \approx 0.6$, $\lambda(c)$ goes to 0.

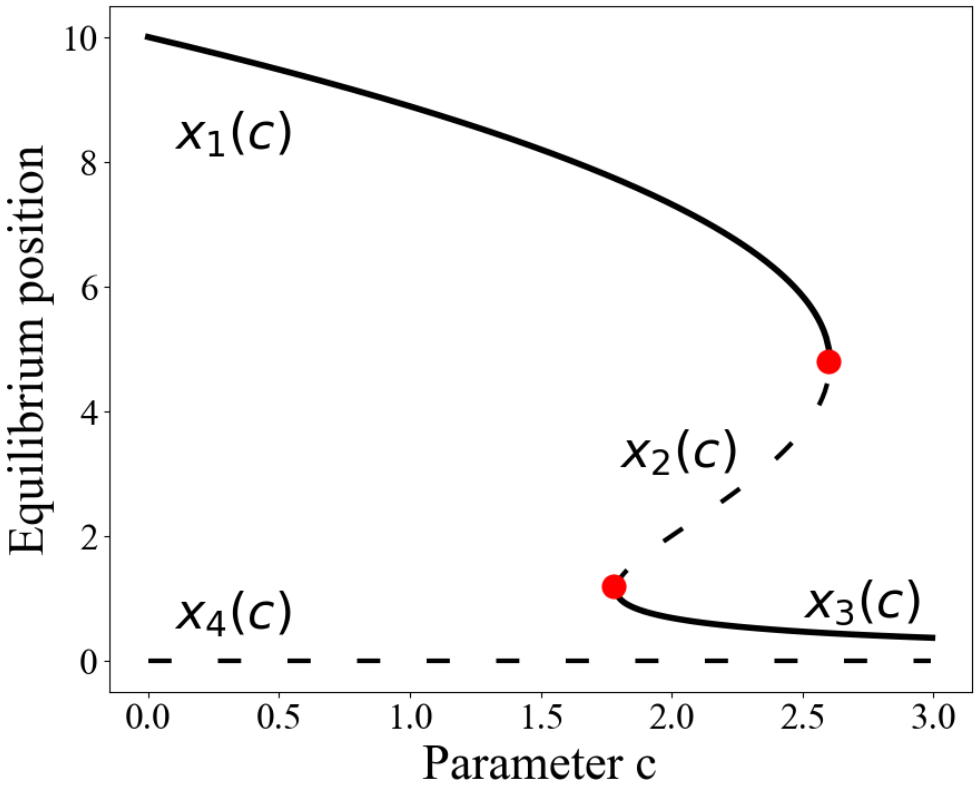


Figure 3.1: One-parameter bifurcation diagram in the (c, x)-plane. Solid lines denote the stable equilibria, dashed lines denote the unstable equilibria. For different values of c. K =10

As the linearised HP system in Eq. (3.2) is in the form of an Ornstein-Uhlenbeck (OU) process [7], its probability density function can be calculated by solving the respective 'Fokker-Planck' equation using the methods in textbooks such as [7]. As a result, analytical formulas for the expected value, variance and autocorrelation of the system, as defined in [7], can be derived and are given

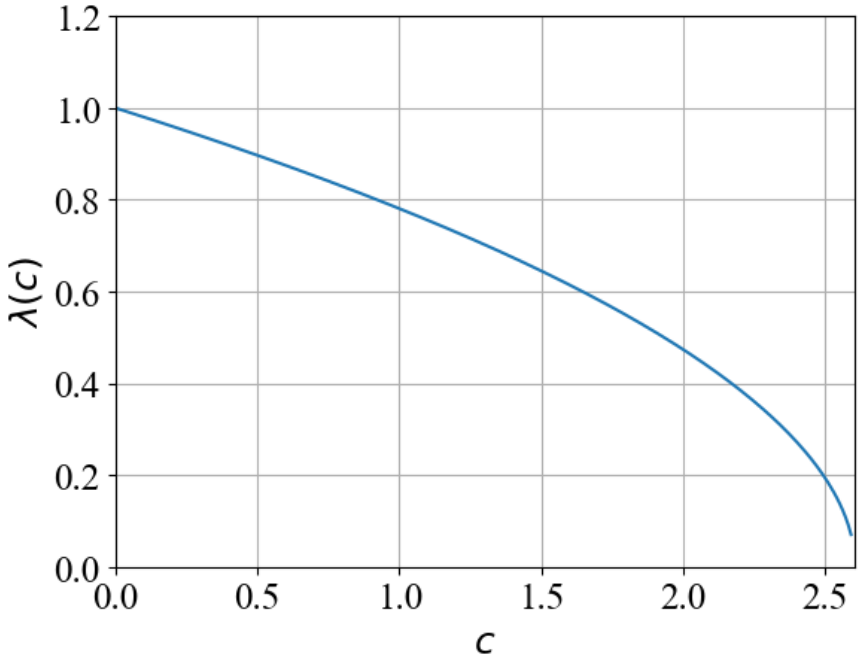


Figure 3.2: Graph of the eigenvalue of the linearised HP system over c for $K = 10$.

below:

$$\langle \bar{x} \rangle = x_1(c), \tag{3.3}$$

$$var\{\bar{x}\} = D/(2\,\lambda(c)), \tag{3.4}$$

$$a_corr\{\bar{x};\tau\} = exp(-\lambda(c)\,\tau), \tag{3.5}$$

where $x_1(c)$ is the upper branch of stable equilibria of the HP system as shown in Figure 3.1.

Numerical simulations

For this example, we fix c at different values ranging from 1 to 2.4, with a step of 0.1, and initialise the HP system at the corresponding $x_1(c)$ values from the branch of fixed points, as shown in Fig. 3.1. Solutions of the HP and linearised HP systems are computed using a Euler-Maruyama method [7] with step size $\Delta = 0.01$ from $t = 0$ to $t_f = 5000$ and $D = 0.2$. In Appendix 6.4.2, we show how

we calculated this.

We denote as

$$\hat{\mathbf{x}} = \hat{x}_0, \hat{x}_1, \ldots, \hat{x}_N$$

the solution of the system using the Euler-Maruyama method, with $N = t_f/\Delta$. We then examine the evolution of these systems at the c values specified above. In our analysis we estimate the expected value of the state of a given system, $\langle\hat{\mathbf{x}}\rangle$, as the mean value of all states of the system during the simulation. The corresponding 'estimated variance', $var\,\{\hat{\mathbf{x}}\}$, and 'estimated autocorrelation', $a_corr\,\{\hat{\mathbf{x}}, \tau\}$, of the state of the HP and linearised HP systems over time are also computed the same way:

$$\langle\hat{\mathbf{x}}\rangle = \frac{1}{N+1}\sum_{i=0}^{N}\hat{x}_i \tag{3.6}$$

$$var\,\{\hat{\mathbf{x}}\} = \frac{1}{N+1}\sum_{i=0}^{N}(\hat{x}_i - \langle\hat{\mathbf{x}}\rangle)^2, \tag{3.7}$$

$$a_corr\,\{\hat{\mathbf{x}}, \tau\} = \frac{\sum_{i=\tau}^{N}(\hat{x}_i - \langle\hat{\mathbf{x}}\rangle)(\hat{x}_{i-\tau} - \langle\hat{\mathbf{x}}\rangle)}{var\,\{\hat{\mathbf{x}}\}}. \tag{3.8}$$

We refer to this values as the estimated mean, estimated variance and estimated autocorrelation. The estimated mean also represents the estimated position of the equilibrium of the noise-free system. The delay term τ is also referred as the 'lag' (where $lag = \tau/\Delta$). While τ is in units of the HP system, lag is an integer that counts the delay in terms of time steps passed. We also write a_corr in terms of lag as $a_corr\,(lag)\{\hat{\mathbf{x}}\} = a_corr\{\hat{\mathbf{x}}, lag\}$.

Note : As it is expected, when we perform the Euler-Maruyama method on the HP systems, some of the solutions may cross the branch of the unstable equilibria $x_2(c)$ and evolve closer to the $x_3(c)$ branch, instead of the original $x_1(c)$. To accurately estimate the variance and autocorrelation of the system close to the equilibrium of the noise-free system that is located in the $x_1(c)$ branch, we discard solutions that have the above behaviour.

In Figs. 3.3, 3.4 and 3.5, we see the $\langle \hat{\mathbf{x}} \rangle$, $var\{\hat{\mathbf{x}}\}$ and $a_corr\{\hat{\mathbf{x}}, \tau\}$ for the HP and linearised HP systems, for the specified c values. Moreover, in the same figures we plot the theoretical values of these measures for the linearised HP system, calculated using the Eq. (3.3),(3.4) and (3.5) As we can see, the estimated values calculated using the numerical solutions match the theoretical values of the linearised HP system and showcase a clear change (increase) in variance and autocorrelation as the bifurcation parameter c gets closer to the bifurcation point.

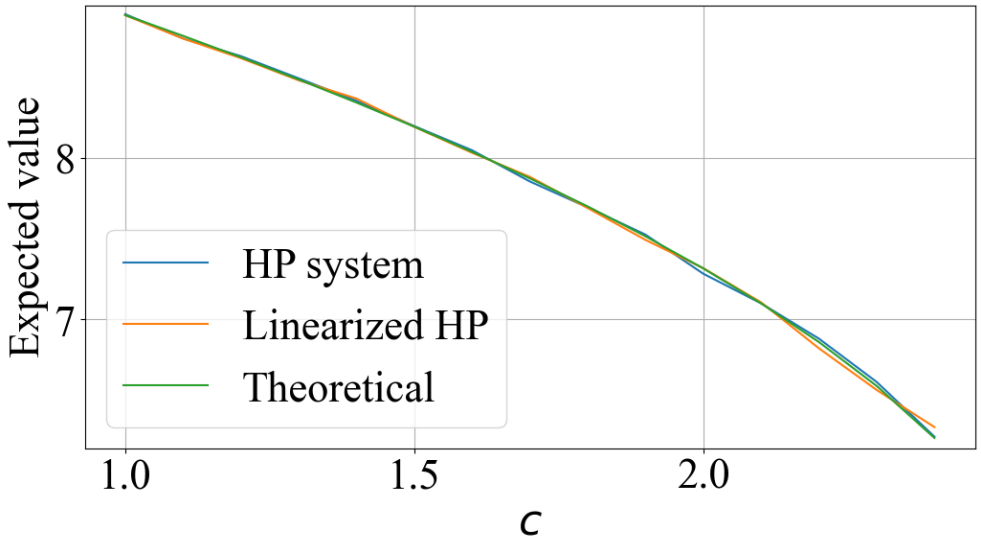


Figure 3.3: Estimated positions of the equilibrium of the HP system (Eq. (3.1)), the linearised HP system (Eq. (3.2)), and their expected values given by Eq. (3.3). K =10, D = 0.2

3.1.2 Early warning signals in epileptic seizures

In [12], Milanowski and Suffczynski use the metrics of variance and autocorrelation, based on the work of Scheffer et.al. in [16], to study the existence of characteristic behaviours prior to epileptic seizures in adults. The main characteristic feature of seizure dynamics is the existence of evolving oscillations that

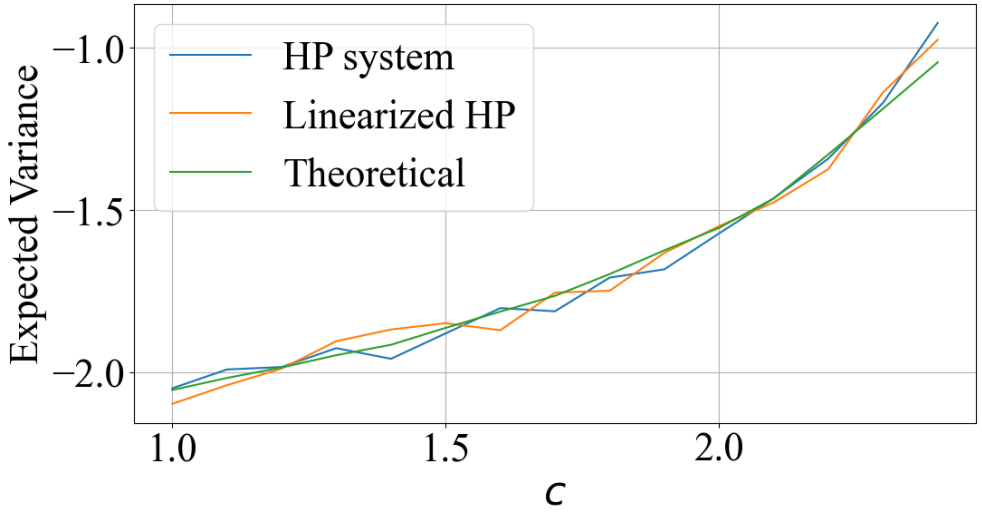


Figure 3.4: Estimated variance of the HP system (Eq. (3.1)), the linearised HP system (Eq. (3.2)), and their expected values given by Eq. (3.4). K =10, D = 0.2

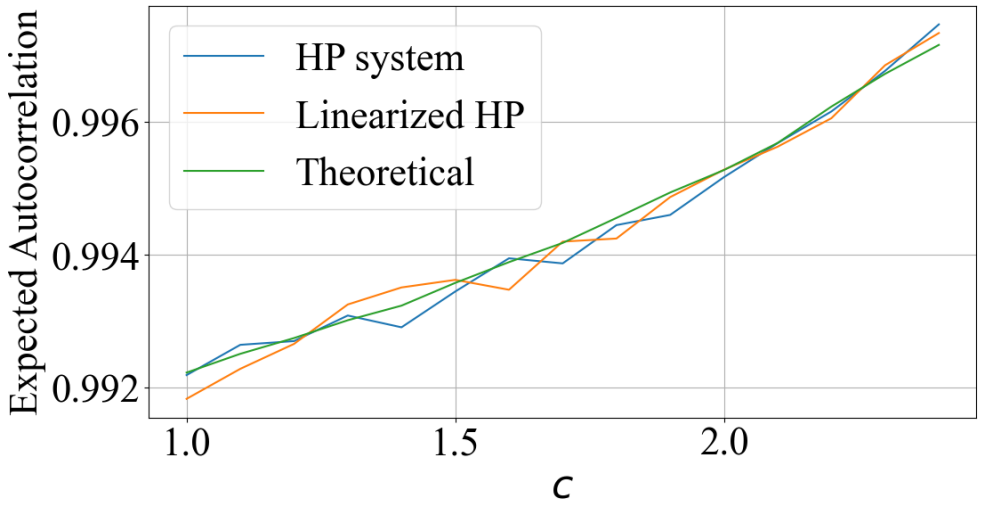


Figure 3.5: Estimated autocorrelations of the HP system (Eq. (3.1)), the linearised HP system (Eq. (3.2)), and their expected values given by Eq. (3.5). K =10, D = 0.2, lag = 1.

begin abruptly and gradually fade away. A simple way to describe this be-

haviour locally is via a Hopf bifurcation, like the examples studied in [12]. In their work, Milanowski and Suffczynski investigate whether a Hopf bifurcation in a particular dynamical system quantifies the system's "critically slowing down" behaviour that is associated with a critical transition taking place. In [12], the authors carry out a dynamic analysis of their model, using a rolling variance and rolling autocorrelation technique and they showcase that we expect an increase in variance and autocorrelation as their system undergoes three different types of bifurcations: subcritical Hopf, supercritical Hopf and "broken" limit cycle. Finally, Milanowski and Suffczynski demonstrate that although in certain types of epileptic seizures in adult humans similar early warning signals appear, there is no common signature present amongst all seizure recordings. Based on this, we apply similar tools to the INFANT dataset without assuming that a Hopf bifurcation is responsible for triggering the transition to a seizure state.

3.2 Feature Estimation Methods

Various methods exist to estimate the evolution of variance and autocorrelation in an dynamic system. Milanowski in [12] used unweighted rolling window techniques to estimate these measures. In our analysis, we used weighted rolling window techniques and incremental methods to obtain more accurate estimates of the evolution of variance in the EEG recordings. During the preprocessing of EEG signal, as described in Section 2.2, the band pass filter we apply detrends the data. For this reason, we consider the mean of the filtered EEG recordings to be zero everywhere. For our analysis we implement three feature estimation methods. The "Gaussian weighted variance" ($G.Var$) and the "Exponential weighted variance" ($E.Var$) that estimate the variance of the system and the "rolling autocorrelation" (a_corr) that estimates the autocorrelation of the system.

We refer to the $G.Var$, $E.Var$ and rolling a_corr as the 'feature estimation methods', where each method produces a time series describing how the given quantities evolve over time. The parameters that are related to each feature estimation method are given in Table 3.1. These parameters are called the "feature estimation method parameters" and their meaning is explained in the sections below.

Table 3.1: Feature estimation method parameters for each feature estimation method.

Method	Parameters
$G.Var$	w_v
$E.Var$	w_e
a_corr	w_a, lag

Note that EEG recording are discrete signals. This means that the methods presented below focused on the analysis of discrete data. For the purposes of this section, we will consider the time step size of the sampling to be Δ. Additionally, for this section, we use $x(t)$ to denote the value of the data at time t, for $t = 0, \Delta, \ldots$.

3.2.1 Gaussian weighted variance

To estimate the var at each time step of the EEG recordings, we implement two different methods. The first method we use is a 'Gaussian rolling variance' (G.Var), which is a weighted rolling window technique of size w_v seconds where each point inside the window is weighted based on a truncated Gaussian distribution with mean $= \mu$ equal to the time at the middle of each given window and a variance of σ^2, where $\sigma = w_v/6$. The distribution is truncated in the interval $[\mu - 3\sigma, \mu + 3\sigma]$ such that 99.73% of the distribution is inside the given window.

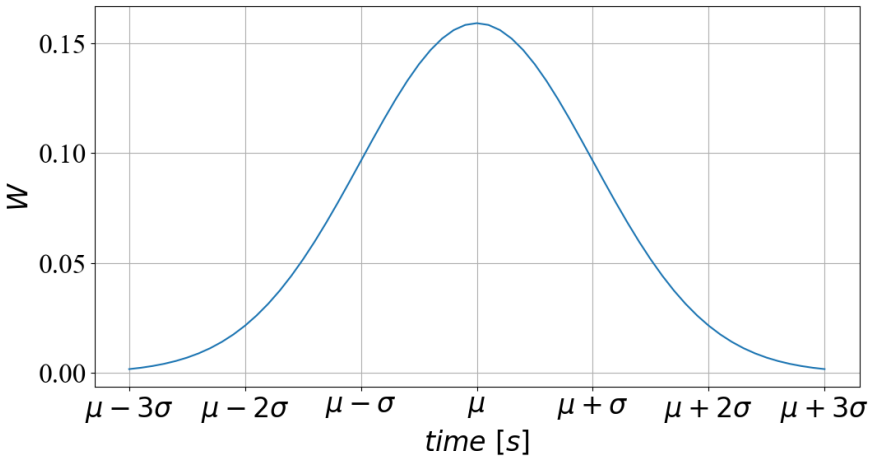


Figure 3.6: Weights used in the calculation of the G.Var at time $t = \mu$ using a window size of $w_v = 6\sigma$.

We calculate the Gaussian weighted variance as follows:

$$G.Var(x,t) = \frac{1}{2N+1} \sum_{\tau=-N}^{N} W(t+\tau)x(t+\tau)^2 \tag{3.9}$$

where $\tau = -N, -N+\Delta, \ldots, -\Delta, 0, \Delta, \ldots, N-\Delta, N$, $N = 3\sigma$, $\mu = t$, $\sigma = w_v/6$ and the values of $W(\tau)$ are given by the graph shown in Fig. 3.6.

For this method, if we consider $x(t)$ defined for $t = 0, \Delta, \ldots, N$, then $G.Var(x,t)$ is defined for $t \in [w_v/2, N - w_v/2]$. The implementation of this method is shown in Appendix 6.3.1. For further information on 'rolling window techniques, see [22].

3.2.2 Exponential weighted variance

The second method that we use is an 'exponential weighted variance' (E.Var), which is an incremental method where the variance of a detrended time series x

at time t is calculated as,

$$E.Var(x,t) = (1-h)(E.Var(x,t-\Delta) + h\,x(t)^2), \tag{3.10}$$

$$E.Var(x,0) = (1-h)hx(0)^2 \tag{3.11}$$

where $t = 0, \Delta, \ldots$ and $h = 1 - 0.1^{\frac{1}{w_e/\Delta+1}}$ and $w_e > 0$. This approach is a special case of a weighted variance, which uses all the history of the system until the current time t and weights the history of the given measurements based on a discretised truncated exponential distribution. Here w_e is related to the time interval $[t - w_e, t]$, such that for large t, 90% of the weights of the method fall within this time interval. For this reason, even though this method uses all the history of the system, we call w_e the window interval length. The implementation of this method is shown in Appendix 6.3.2.

We can rewrite Eq. (3.10) in the form of a sum as follows:

$$E.Var(x,t) = \frac{1}{t}\sum_{\tau=0}^{t} W(\tau;t)x(\tau)^2 \tag{3.12}$$

where $\tau = 0, \Delta, \ldots, t$ and $W(\tau;t)$ are the weights used at time t as shown in Figure 3.7. More detailed analysis of the $E.Var$ and how the formula for h is calculated is given in Appendix 6.1.1.

3.2.3 Rolling autocorrelation

Finally, we employ an unweighted rolling window technique of window size w_a seconds and delay lag steps to estimate the autocorrelation. This technique, which we call 'rolling a_corr', provides an estimate of the evolution of a_corr over a given time interval $[t - w_a, t]$. The formula for calculating the a_corr is

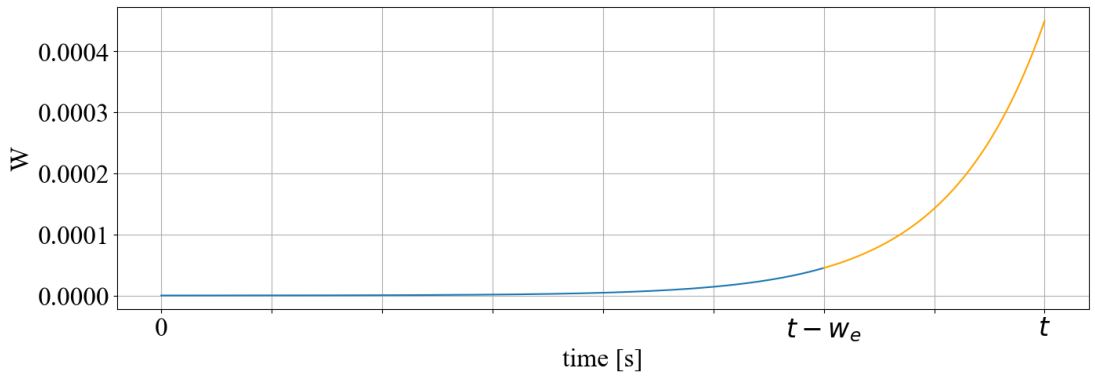


Figure 3.7: Weights used in the calculation of the E.Var at time $t = 80s$ using a window size of $w_e = 20s$, $\Delta = 1/256$. Blue: weights outside $[t - w_e, t]$. Orange: weights inside $[t - w_e, t]$.

given by:

$$a_corr(x, t_0; w_a, lag) = \rho(X_+, X_-), \tag{3.13}$$

$$X_+ = [x(t_0 - w_a), x(t_0 - w_a + \Delta), \ldots, x(t_0 - lag\ \Delta)], \tag{3.14}$$

$$X_- = [x(t_0 - w_a + lag\ \Delta), x(t_0 - w_a + (lag + 1)\Delta), \ldots, x(t_0)], \tag{3.15}$$

where $lag \in \mathbb{N}$ and $\rho(X, Y)$ is the Pearson correlation coefficient of the time series X and Y calculated as:

$$\rho(X, Y) = \frac{\sum_{i=0}^{N} x_i y_i}{\sqrt{\sum_{i=0}^{N} x_i^2 \sum_{i=0}^{N} y_i^2}}, \tag{3.16}$$

for $X = (x_0, x_1, \ldots, x_N)$ and $Y = (y_0, y_1, \ldots, y_N)$. Remember, we are considering the data to be detrended, meaning that their mean is considered to be zero. The implementation of this method is shown in Appendix 6.3.3.

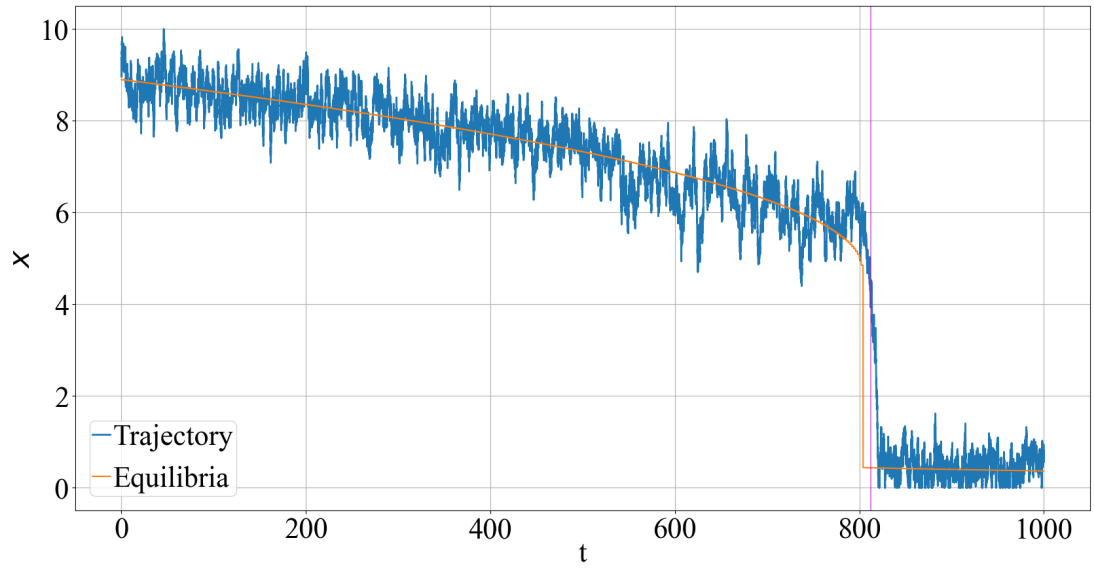


Figure 3.8: Simulated trajectory (blue) of system (3.1) and the trajectory of the attractor (orange). Magenta lines: time of the critical transition.

Example (Part Two): Dynamic analysis of the Harvested Population system

For the dynamic analysis, where $c = c(t)$ varies over time, the HP system is initialised at the same $x_1(c)$ as before with $c(t_0) = 1$ and $t_0 = 0$ and c is designed to grow linearly with a drift rate of $v_c = 0.0004$ per unit of time until $c(t_f) = 3$ where $t_f = (c(0) - c(t_f))/v_c = 1000$. Solutions of the HP system are computed using the Euler-Maruyama method with step size $\Delta = 0.05$. Based on the bifurcation diagram from Fig. 3.1, the HP system will undergo a critical transition due to a saddle-node bifurcation at $c \approx 2.6$, which corresponds to the time $t_b \approx 800$. Fig 3.8 shows an example of a trajectory of the HP system along with the respective equilibrium at each time step.

For the calculation of $G.Var$, $E.Var$ and a_corr we need to remove the mean of the system in advance. We do this using a weighted rolling window technique

similar to $G.Var$ which we call the "Gaussian rolling average" ($G.Av$). The formula the estimates the mean of the system at time t, using a window size of w_m, is:

$$G.Av(x,t) = \frac{1}{2N+1} \sum_{\tau=-N}^{N} W(t+\tau)x(t+\tau) \tag{3.17}$$

where $\tau = -N, -N+\Delta, \ldots, -\Delta, 0, \Delta, \ldots, N-\Delta, N$, $N = 3\sigma$, $\mu = t$, $\sigma = w_m/6$ and the values of $W(\tau)$ are calculated similarly with the $G.Var$ as shown in Fig. 3.6 before. Similar to $G.Var$, if we consider $x(t)$ defined for $t = 0, \Delta, \ldots, N$, then $G.Av(x,t)$ is defined for $t \in [w_m/2, N - w_m/2]$. With these techniques, we remove the mean from the simulated data as

$$\hat{x}(t) = x(t) - G.Av(x,t)$$

defined on the same time interval as $G.Av$, $t \in [w_m/2, t_f - w_m/2]$.

Then, we calculate $G.Var$, $E.Var$ and a_corr, as defined in Section 3.2, using window sizes $w_m = w_v = w_e = w_a = 100s$ and $lag = 1, 3$ and 5. Figures. 3.9 and 3.10 show that prior to the critical transition (located at the vertical magenta line in each plot), the var and a_corr begin to increase.

The choice of the window size and the lag influences the accuracy and the resulting increase or decrease of variance and autocorrelation prior to the critical transition. We showcase the effect of the window size selection by performing 1000 simulations for $t_f = 1000$, $c(0) = 2$, $c(t_f) = 2.4$, $D = 0.2$, two different sets of window sizes, $w_m^1 = w_v^1 = w_e^1 = w_a^1 = 10s$, $w_m^2 = w_v^2 = w_e^2 = w_a^2 = 50$, $lag = 1$ and $\Delta = 0.001$. As $c(t_f)$ is before the bifurcation point, we reject simulations that cross the unstable equilibrium $x_3(c)$ as shows in Figure 3.1 and generate a new one until 1000 simulations have been completed. For these simulations, we remove the mean, calculate the $G.Var$, $E.var$, a_corr and we calculate a linear fit over the outcome of the $G.Var$, $E.Var$ and a_corr. Then, we enumerate the amount of simulations whose linear fit have a positive or a negative slope, for

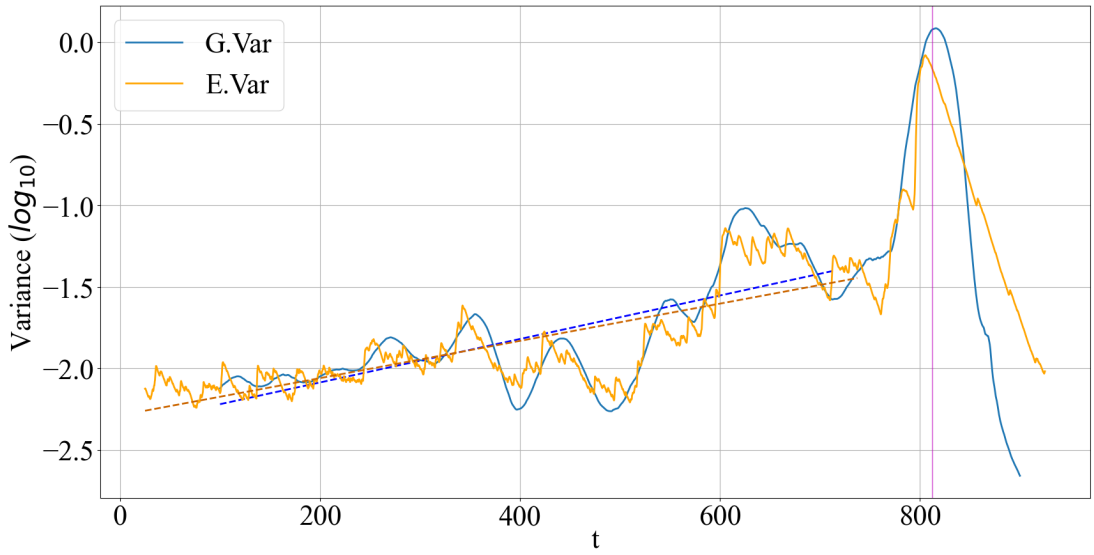


Figure 3.9: The variance of the system (3.1) using G.Var (solid blue) and E.Var (solid orange), along with the linear fit for the time interval prior to the critical transition (dashed lines). Magenta lines: time of the critical transition.

each method. The result of the amount of positive and negative slopes is shown in Table 3.2.

We observe from Table 3.2 that for the window size of $10s$, the ratio of positive to negative slopes is approximately $2:1$ while for window size $50s$, the ratio increases to $9:1$. This shows clearly that the choice of window sizes heavily impacts whether we observe an increase in variance and autocorrelation prior to the bifurcation point, over all the simulations. Thus, in our study, we perform a parametric analysis over various window sizes and *lag*s and we choose those which produce the best ratio of positive to negative slopes, as we explain in the next sections.

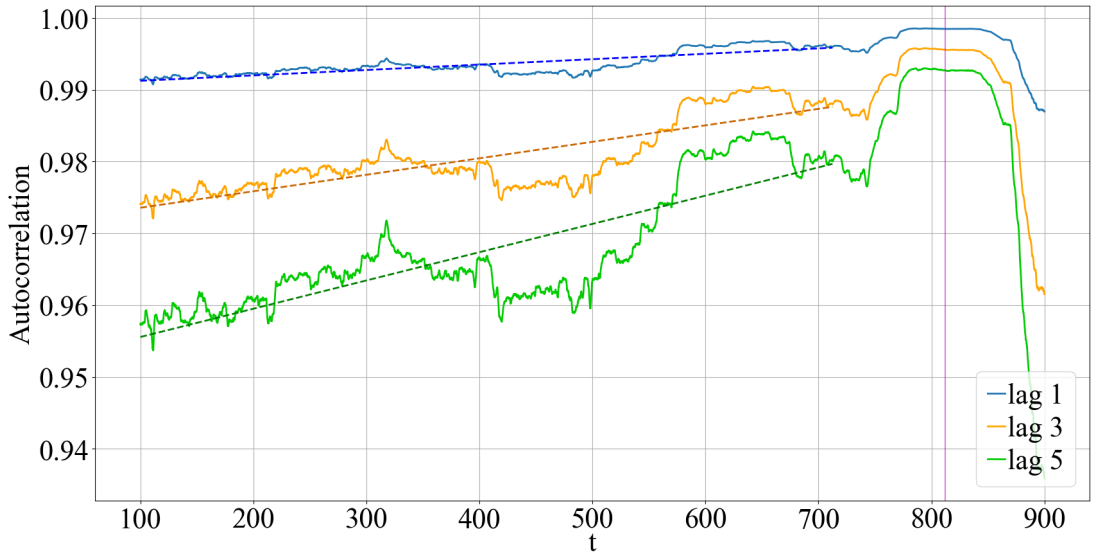


Figure 3.10: The autocorrelation of the system (3.1) using rolling $a_corr(lag)$ for lag 1 (solid blue), 3 (solid orange) and 5 (solid green), along with the linear fit for the time interval prior to the critical transition (dashed lines). Magenta lines: time of the critical transition.

Table 3.2: Number of positive/negative slopes for $G.Var$, $E.Var$ and a_corr for the HP system when c varies from 2 to 2.4 for window sizes $w^1 = 10s$ and $w^2 = 50s$.

Method	Pos/Neg w^1	Pos/Neg w^2
$G.Var$	685 / 315	907 / 93
$E.Var$	697 / 303	918 / 82
a_corr	701 / 299	909 / 91

3.2.4 Measure of statistical significance of binary indicators

The authors of the studies [12, 16] state that positive or negative changes in variance and autocorrelation should be expected prior to the bifurcation point. However, unless we are aware of the underlying system, the theory is unable to provide an expected rate of change of the variance and autocorrelation. Therefore, in [12], the authors do not take into account the rate of change of variance and autocorrelation prior to the seizure onsets; instead, they bases their conclusions only on the existence of an increase or decrease preceding a seizure.

Keeping in line with this methodology, we employ a binary indicator based on the increase or decrease in variance or autocorrelation prior to the onset of a seizure, ignoring the rate at which this change occurs. We do this by performing a linear fit over the variance and autocorrelation data prior to a seizure, and we use the sign of the slope as the binary indicator. What this means is that, after calculating the feature estimation methods, we perform a linear fit over a given time interval prior to the seizure and we use the sign of the slope that we calculate in the linear fit as a binary indicator. The implementation of this method is shown in Appendix 6.2.2.

In order to determine the statistical significance of a binary indicator, such as the presence of a characteristic increase or decrease prior a seizure, we perform a binomial test. By means of this test, we are able to determine the probability that the distribution of the binary indicator values (increase / decrease) we calculate prior to the onset of the selected seizures for a given neonate, is the same as the distribution of a series of Bernoulli trials with a success rate of 50%. The probability that the true distribution of increases and decreases prior to the start of a seizure is as extreme as that of a sequence of Bernoulli trials is indicated by the p-value of the binomial test. Therefore, the greater the significance of the

indicator, the smaller the p-value. In general, the value of the threshold that determines if the p-value is significant small is chosen arbitrarily based on the amount of data used, the field of study and more.

Note : In our analysis we focus on the detection of possible binary indicators. We draw our indicators from theoretical models and expected behaviours of a critical transitions. Normally, we would like to test these indicators in time intervals that are prior to seizures and time intervals that are not close to any seizure events. This way, we can test whether the characteristic behaviour we detect is unique to onset intervals or can be found throughout the EEG recording. In our analysis we only focus on finding the indicators from the theoretical models and test them in time onset intervals. This means that even if the binary indicator shows that there exists a characteristic behaviour, we still need to check if the characteristic behaviour is unique to onset intervals. This part is not included in this study.

3.2.5 Finding 'optimal' feature estimation method parameters

In [12], Milanowski and Suffczynski demonstrate the feature estimation methods they use for detecting the onset of seizures only for selected rolling window sizes and lag, but they do not showcase how these parameters are selected. In our analysis, we carry out a parametric study to determine which sets of values of the feature estimation method parameters, namely the w_v, w_e, w_a and lag, that produce the most significant results for each feature estimation method, namely the $G.Var, E.Var$ and a_corr.

To do this, we apply the feature estimation methods described in Sec. 3.2 to all studied intervals according to the criteria discussed in Sec. 2.3 and conduct an analysis over a range of 'onset interval lengths'. In our parametric study,

we consider 'onset interval lengths' from 4 to 40 seconds (in steps of 1 second), lengths of window sizes, for each feature estimation method independently, from 1 to 19 seconds (in steps of 2 seconds) and the lag which ranges from 1 to 127 (in steps of 2 lags).

Note : There is a significant difference between the notions of a studied interval and an onset interval. The studied intervals, which are introduced in Sec. 2.3, are 60 seconds time intervals prior to a selected seizure that are used to calculate the estimated var and a_corr using the feature estimation methods. These studied intervals are used for the calculation of $G.Var, E.Var$ and a_corr. An onset interval denotes a sub-interval of the studied interval and is used to calculate the linear fit over the estimated var and a_corr prior to a seizure. The onset interval can be different for each method, $G.Var, E.Var$ and a_corr. In Fig3.11, we show an example where the full 60 seconds of studied interval in the top graph (in solid green) and the onset intervals for each feature estimation method in the second third and forth graph (in solid orange). The linear fits are shown in dashed orange.

As the first step of our analysis, for each neonate, we divide the set of the selected seizures randomly into two subsets: a) the 'training set' consisting of $\approx 80\%$ of the seizures and is used to find the parameters that produce the most 'significant' results and b) the 'test set' consisting of $\approx 20\%$ of the seizures that we use to verify the significance of the results from the training set. This technique of separating the data in training and test set is one case of "cross-validation statistical test".

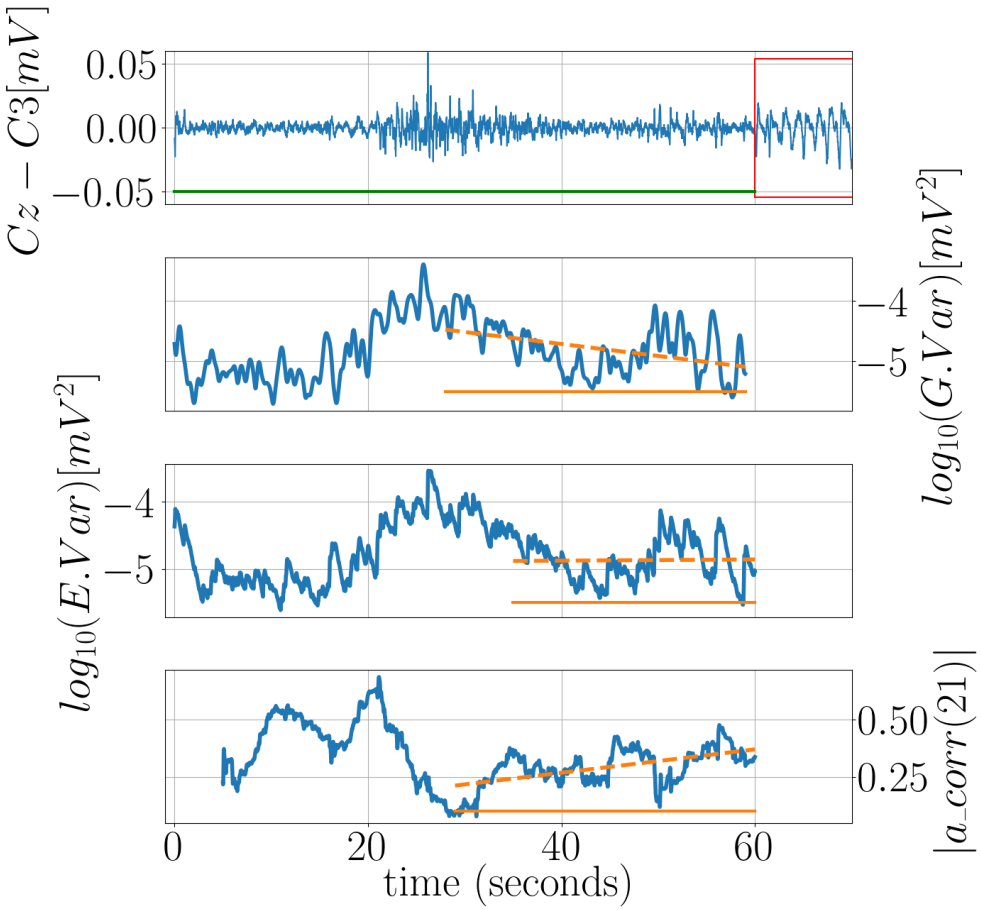


Figure 3.11: Example of EEG data from Neonate 3 along side the calculated $G.Var, E.Var$ and a_corr over the studied time interval of 60 seconds (solid green) and the linear fit (dashed orange) calculated on $G.Var, E.Var$ and a_corr over the onset interval (solid orange) for each method. Onset interval lengths are : $G.Var$ - 31 seconds, $E.Var$ - 25 seconds, a_corr - 31 seconds. Red box: seizure intervals as annotated by experts.

In our analysis, we aim to find possible characteristic behaviours prior to a seizure event. To achieve this, we implement the feature estimation methods, namely $G.Var$, $E.Var$ and a_corr, to the selected studied intervals. Then, for various sets of window sizes, lag and onset interval lengths, we check in how many

of the studied intervals we observe an increase or a decrease prior to the seizure, based on the training set. If the difference between the amount of increases and decreases we observed is significant enough, we check if, for the same parameters that the behaviour is observed, the behaviour persists on the training set. The steps we follow to achieve this are stated below:

1. Implement the feature estimation method on the training set of studied intervals.

    - Perform this step for each values of window size. For the calculation of the a_corr we consider $lag = 1$.

2. For each outcome of Step 1, we perform a linear fit over the onset interval lengths.

    - Perform this step for each values of onset interval length.

3. For each set of onset interval length and window size, we perform a binomial test on the sign of the slopes on the linear fits.

4. Fix the onset interval length and window size to the values that give the smaller p-value in Step 3.

5. If the feature estimation method is the a_corr:

    (a) We implement the feature estimation method on the training studied intervals, again.

        - Perform this step for each values of lag. We keep the window size equal to the selected value from Step 4.

    (b) For each outcome of Step 5(a), we perform a linear fit over the fixed onset interval lengths.

(c) For each *lags*, we perform a binomial test on the sign of the slopes on the linear fits.

(d) Fix *lag* to the values that give the smaller p-value of the Step 5(c).

6. If the p-value we get is greater than 10^{-3}, we say that no characteristic behaviour found. If the p-value we get is less than 10^{-3}, we continue to the next steps.

7. We implement the feature estimation method on the test set using the fixed window size and lag, if applicable.

8. We perform a linear fit using the fixed onset interval length.

9. We perform a binomial test on the sign of the slop of the linear fit.

10. If the p-value we get is greater than 0.2, we say that no characteristic behaviour found. If the p-value we get is less than 0.2, we say that this feature estimation method detects a potential characteristic behaviour.

Using the above steps, we are able to check if the feature estimation methods we selected can detect a potential characteristic behaviour prior to a set of seizure onsets. In the next chapter, we implement the above steps to the three selected neonates and discuss the conclusions we draw from the results of the analysis.

Chapter 4

Results

4.1 Early warning signals on HIE seizure onsets

In this section, we present the optimal feature estimation method parameters, calculated based on the methodology explained in section 3, for the Neonates 3, 10 and 13. The minimal feature estimation method parameters and the minimal onset interval length, for each feature estimation method are specified in Tables 4.1, 4.2 and 4.3, for the three neonates respectively. The fifth column in these Tables shows the number of positive/negative slopes that are calculated based on the minimal parameters, and the sixth column contains the p-value of the binomial test performed to measure the statistical significance of the results using the 'training set'.

Table 4.1: Minimal parameters for each feature estimation method for Neonate 3.

Method	Window size [s]	lag	Onset interval length [s]	Pos./Neg. slopes	p-value
G.Var	1	-	31	84/39	$6.0 \cdot 10^{-5}$
E.Var	3	-	25	82/41	$27 \cdot 10^{-5}$
$\lvert a_corr \rvert$	5	21	31	41/82	$27 \cdot 10^{-5}$

Table 4.2: Minimal parameters for each feature estimation method for Neonate 10.

Method	Window size [s]	lag	Onset interval length [s]	Pos./Neg. slopes	p-value
G.Var	1	-	32	88/22	$1.5 \cdot 10^{-10}$
E.Var	1	-	32	86/24	$2.2 \cdot 10^{-9}$
$\lvert a_corr \rvert$	1	13	14	31/79	$5.3 \cdot 10^{-6}$

Table 4.3: Minimal parameters for each feature estimation method for Neonate 13.

Method	Window size [s]	lag	Onset interval length [s]	Pos./Neg. slopes	p-value
G.Var	19	-	10	62/37	0.01
E.Var	19	-	4	28/70	$2.6 \cdot 10^{-5}$
$\lvert a_corr \rvert$	11	81	14	65/33	10^{-3}

Table 4.4: Positive/Negative slopes and the p-value of a binomial test for the minimal parameters based on the 'test set' of Neonate 3.

Method	Pos./Neg. slopes	p-value
G.Var	18/10	0.18
E.Var	19/9	0.09
$\lvert a_corr \rvert$	7/21	0.01

Table 4.5: Positive/Negative slopes and the p-value of a binomial test for the minimal parameters based on the 'test set' of Neonate 10.

Method	Pos./Neg. slopes	p-value
G.Var	25/3	$2.7 \cdot 10^{-5}$
E.Var	25/3	$2.7 \cdot 10^{-5}$
$\lvert a_corr \rvert$	10/18	0.18

Table 4.6: Positive/Negative slopes and the p-value of a binomial test for the minimal parameters based on the 'test set' of Neonate 13.

Method	Pos./Neg. slopes	p-value
E.Var	9/16	0.22
$\lvert a_corr \rvert$	14/11	0.69

For Neonates 3 and 10, the binomial test performed, using the minimal parameters, resulted in p-values lower than 10^{-3} for all feature estimation methods. Tables 4.4 and 4.5 shows the positive/negative slopes and the corresponding p-value of the binomial test performed over the test set using the corresponding minimal parameters. All feature estimation methods shows p-values less than 0.2 for both Neonates 3 and 10, meaning that there is a characteristic behaviour prior to a seizure. Thus, the parameters in Tables 4.1 and 4.2 are considered the optimal ones based on the data used in our analysis.

For Neonate 13, the binomial test performed, using the minimal parameters, resulted in p-values lower than or equal to 10^{-3} only for the E.Var and $|a_corr|$ methods. Table 4.6 shows the resulting positive/negative slopes and the corresponding p-value of the binomial test performed over the test set using the corresponding minimal parameters. The corresponding p-value for the E.Var and the $|a_corr|$ methods is greater than 0.2, meaning that the results are insignificant and the minimal parameters are not optimal.

4.1.1 Examples of seizure onsets using the 'optimal' parameters

In this section, we present three examples of seizure onsets from Neonate 3 alongside the results of our analysis using the optimal parameters as shown in Table 4.1. The example in Fig. 4.1 is from the training set, and in Figs. 4.2-4.3 the examples are from the test set of intervals from Neonate 3.

In Fig. 4.2 we provide an example where there is an increase in both the G.Var, the E.Var while the absolute value of the rolling a_corr displays a decrease prior to the seizure. The slopes as calculated based on the optimal feature estimation methods are 0.02 and 0.027 for $G.Var$ and $E.Var$, respectively, and -0.011 for $|a_corr|$.

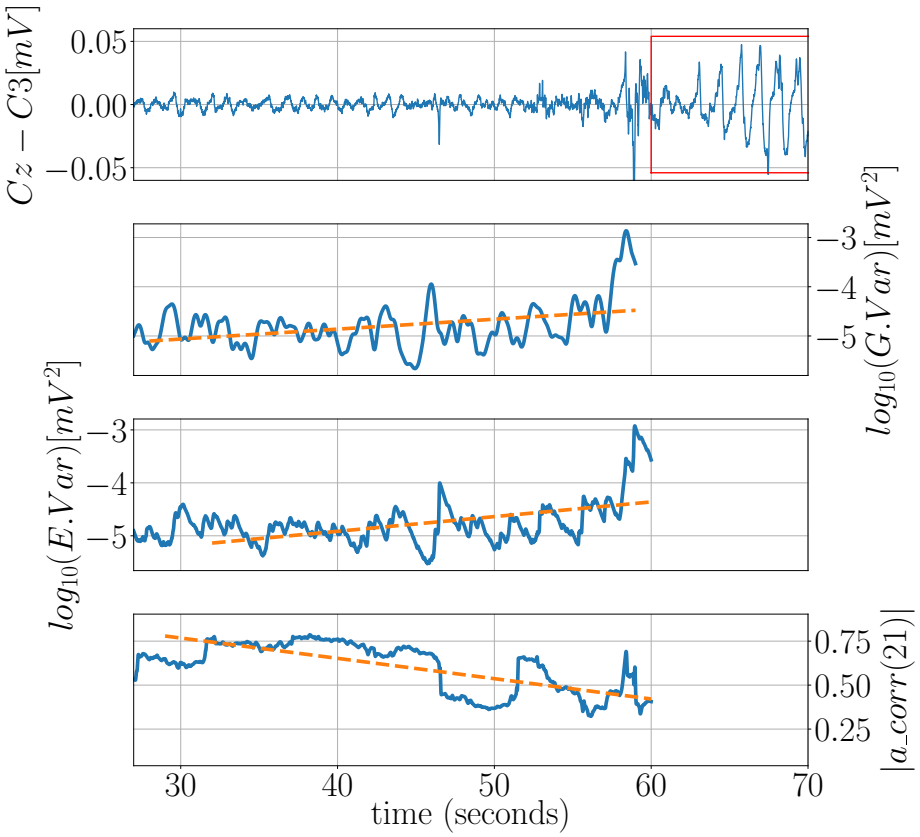


Figure 4.1: Example of EEG recording of a selected interval in the $C_z - C_3$ pair from Neonate 3 and the results of the G.Var, E.Var and rolling $|a_corr|$ analysis based on the parameters given in Table 4.1. Dashed line: linear fit over the optimal onset interval. Red box: seizure interval as annotated by experts.

In contrast, in the example displayed in Fig. 4.3 there is a decrease in the G.Var and E.Var while the $|a_corr|$ shows an increase prior to the seizure. The slopes as calculated by the based on the optimal feature estimation methods are -0.019 and -0.005 for $G.Var$ and $E.Var$, respectively, and 0.05 for $|a_corr|$.

In Fig. 4.1 we provide an example where the G.Var and E.Var displays no change in the slope and the $|a_corr|$ exhibits an increase. The slopes as calculated

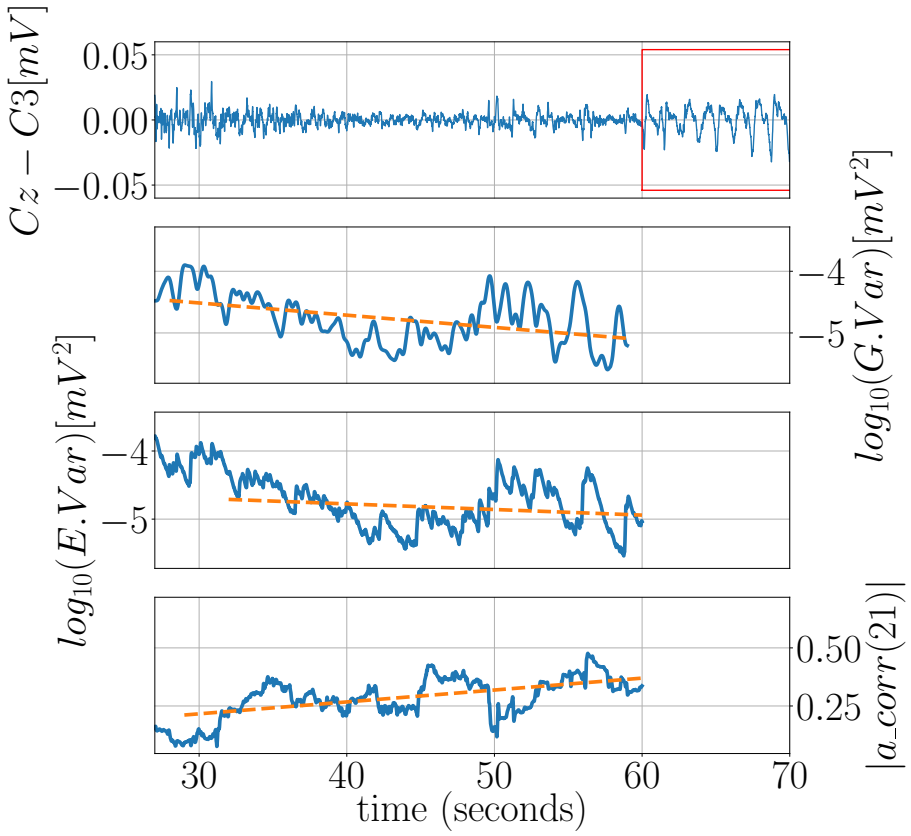


Figure 4.2: Example of EEG recording of a selected interval in the $C_z - C_3$ pair from Neonate 3 and the results of the G.Var, E.Var and rolling $|a_corr|$ analysis based on the parameters given in Table 4.1. Dashed line: linear fit over the optimal onset interval. Red box: seizure interval as annotated by experts.

by the based on the optimal feature estimation methods are 0.0058 and 0.0002 for $G.Var$ and $E.Var$, respectively, and 0.017 for $|a_corr|$.

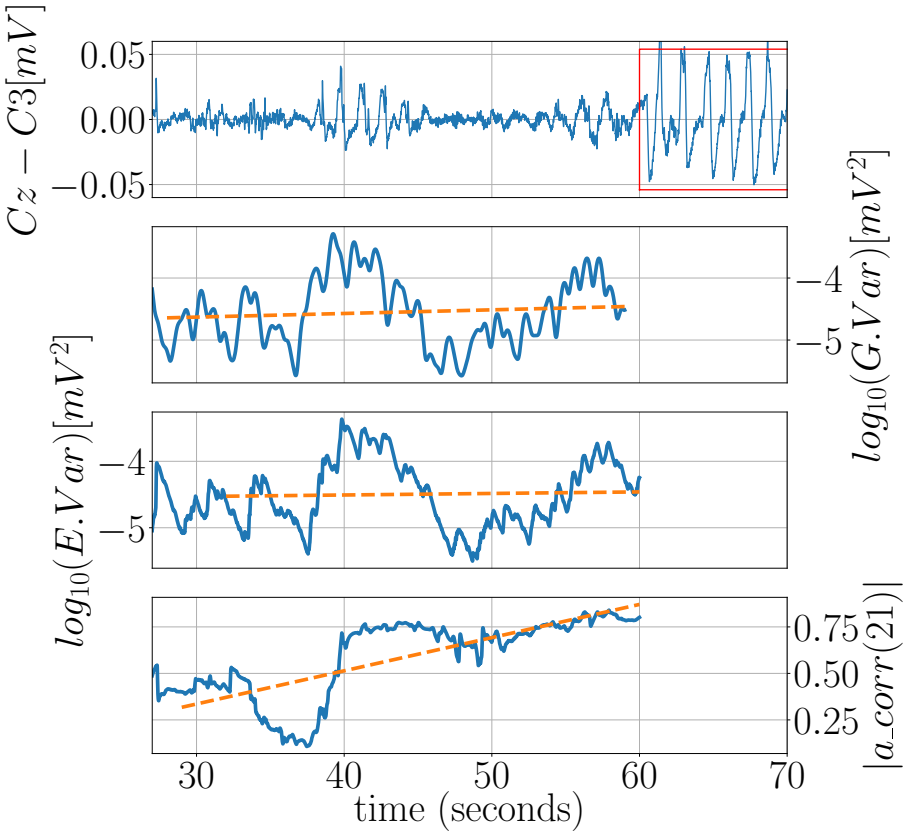


Figure 4.3: Example of EEG recording of a selected interval in the $C_z - C_3$ pair from Neonate 3 and the results of the G.Var, E.Var and rolling $|a_corr|$ analysis based on the parameters given in Table 4.1. Dashed line: linear fit over the optimal onset interval. Red box: seizure interval as annotated by experts.

4.2 Analysis and comparison of the results between the neonates

From the results presented in Section 4.1, our analysis found potential characteristic behaviours for Neonates 3 and 10, but not for Neonate 13. From the metadata provided from the INFANT research Centre for each neonate, which

consists of Sarnat grade, sex, gestational age, weight and more, we were able to identify that Neonate 3 and 10 share the same Sarnat grade (severe), while Neonate 13 has moderate Sarnat grade. Of course, we do not claim that this distinction is the reason that we were able to find potential characteristic behaviours for Neonates 3 and 10 and not for Neonate 13, but it is a possible explanation that is worth to be explored in the future.

From Neonates 3 and 10, Neonate 10 present better results, meaning that the resulting p-values in the training and test set are much lower. This raises the question of whether the optimal values for Neonate 10 can also be used on Neonate 3 to detect the same characteristic behaviour, even if these values are not optimal for Neonate 3. Although the optimal parameters for Neonate 10 are not the optimal for Neonate 3, when we use the optimal parameters of Neonate 10 for Neonate 3, the resulting p-values are on the scale of 10^{-4} and the same characteristic behaviour is observed, increase in variance and decrease in autocorrelation. This implies that by using the following parameter values the same characteristic behaviour is observed in two separate neonates, even though the parameters are obtained using the data from one neonate only: a) window sizes $w_v, w_e, w_a = 1s$ for all three methods, b) for the autocorrelation $lag = 13$, c) onset interval length of $32s$ for the $G.Var$ and $E.var$ and $14s$ of the $|a_corr|$.

Chapter 5

Discussion

Summary

The goal of this study was to analyse the neonatal EEG for INFANT Research Centre and examine the existence of any characteristic behaviour prior to the onset time of brain seizures. The data we use are collected by the INFANT Research Centre in Cork, Ireland and consists of full term neonates that have exhibited symptoms of HIE, based on the Sarnat grade, as explained in Sec. 2. From the dataset, we perform our analysis on three neonates that exhibit a high amount of brain seizures. One has moderate and two have severe Sarnat grade.

Then, we introduced the theory of critical transitions and we select features that can detect characteristic behaviours that take place prior to a critical transition. As the neonatal brain comes closer to a seizure state, we use numerical methods to estimate these features. Finally, we present the steps of the analysis we perform to decide if there exist any characteristic behaviour prior to a seizure event.

Conclusion Based on Sec. 4, we were able to detect a potential characteristic behaviour prior to the seizure in two out of the three neonates we studied. The characteristic behaviour we observed has an increase in variance and a decrease

in the autocorrelation. This behaviour is not consistent with the behaviour we expect prior to a critical transition based on our analysis in Sec.3 and the work done in [12, 16]. However, there are other types of critical transitions that may exhibit the same characteristic behaviour we observed. Hence, more research needs to be done in various types of critical transitions to see if we can identify one with similar behaviour.

The two neonates that we were able to detect a characteristic behaviour, both have severe Sarnat grade, while the third neonate has a moderate Sarnat grade, which indicated lower level of brain damage than the other two. This may be an indication that the characteristic behaviours prior to seizure onsets are more pronounced in neonates with severe Sarnat grade compared to those with mild or moderate Sarnat grade. The amount of data use in our study is not enough to affirm this hypothesis and is left open to be studied next.

Another connection between the two neonates with severe Sarnat grade is similarity in the optimal feature estimation method parameters. This implies that both neonates exhibit similar behaviour prior to a seizure event. Thus, we can consider a single set of parameters to be used for both neonates with severe Sarnat grade. This raises the question whether it is possible to find one set of feature estimation method parameters for all neonates that have severe Sarnat grade. From our analysis and the data used, we propose that using the feature estimation methods presented in Section 3.2, with window sizes of $1s$ for all three methods and $lag = 14$ $(0.05s)$, on EEG recordings from neonates with severe Sarnat grade, we observe a characteristic increase in variance within $32s$ prior to a seizure event and a characteristic decrease in autocorrelation within $14s$ prior to a seizure event.

Limitations

The first limitation of our analysis is the size of our dataset. As we explain in

Sec. 2.3, our analysis is performed on each neonate, separately. For this reason, we can work only with neonates that exhibit enough seizures such that we can perform a cross-validation test. Generally, we need to have more than 130 seizures that satisfy our selection criteria in each neonate we study such that we can perform our analysis. In the dataset we use, only three neonates exhibit enough seizures. This means that our findings needs to be reproduced in more neonates, both within and outside the INFANT research centre.

The second limitation of our analysis, which is also mentioned in Sec. 3.2.4, is that we only study time intervals that are prior to seizures. Due to this limitation in the studied time intervals, we cannot check whether the behaviour we detect is unique to time intervals prior to seizures or can be found throughout the non-seizure EEG data. Thus, after detecting a characteristic behaviour, it is important to measure the ration between the frequency we observe this behaviour prior to a seizure in relation to the frequency we observe the same behaviour to non-seizure related time intervals (time interval that are not close to seizure events). Even though this is not included in our analysis, we recognize its significance. For this reason, we say that our analysis detects potential characteristic behaviours, as it does not check whether the frequency of these behaviours changes prior to seizures.

Future work

Based on the limitations of our analysis, in future research, the number of neonates included in the study should be increased. Also, it is imperative to examine whether the potential characteristic behaviour we observed can be found throughout the EEG recordings. Moreover, based on our results, future research should investigate if the potential characteristic behaviour we identified is common across the neonates with severe Sarnat grade but not those with moderate and mild one.

Finally, neurophysiologists do not consider the prediction of seizures in neonates with HIE significant as it does not affect the treatment of the neonates. The importance of our study is to understand the underline mechanics of the seizure onset and more accurately detect the onset of a seizure. Thus, if the characteristic behaviour we observed can be used to identify the onset of seizures, we can use these features to enhance the future seizure detection algorithms, like the one developed by INFANT Research Centre [21].

The enhancement of seizure identification in the neonatal brain would yield significant advantages in the treatment administered to neonates. Potential effects of this implementation on neonatal treatment include, but are not limited to: a) enhancing the precision of the Sarnat and EEG classifications assigned to the neonate, b) optimizing the initiation and cessation of treatment, and c) reducing the number of active neurophysiologists in a clinic. This elucidates the emphasis on seizure detection in the neonatal brain, a perspective shared by other researchers [1,3,5,12,18].

Chapter 6

Appendix A

6.1 Proofs

6.1.1 Reparametrisation of h

We have rewritten Eq. (3.10) in the form of a sum as follows:

$$E.Var(x,t) = \frac{1}{t}\sum_{\tau=0}^{t} W(\tau;t)x(\tau)^2 \tag{6.1}$$

where $\tau = 0, \Delta, \ldots, t$ and $W(\tau;t) = h(1-h)^{(t-\tau)/\Delta+1}$. We observe that the parameter h determines how fast the weights used for the calculation of $E.Var$ decay. In contrast to the the Gaussian weighted variance method, where the respective parameter w_v represents a window size in seconds, the parameter h is related to the decay rate of the weights.

Our objective is to rewrite h in relation to the parameter w_e which represents a window size in seconds, similarly to the w_v parameter. As $E.Var$ uses all the history of the system, we re-parametrise h such that $p \cdot 100\%$ of the weights are within the time interval $[t - w_e, t]$, for $0 < p < 1$.

From Eq. 6.1, we have that the sum of all the weights is

$$\sum_{\tau=0}^{t} h(1-h)^{(t-\tau)\Delta+1} \overset{s=t-\tau}{=\!=} \tag{6.2}$$

$$\sum_{s=0}^{t} h(1-h)^{s\cdot\Delta+1} \overset{i=s\Delta}{=\!=} \tag{6.3}$$

$$\sum_{i=0}^{t/\Delta} h(1-h)^{i+1} = \tag{6.4}$$

$$(1-h)\sum_{i=0}^{t/\Delta} h(1-h)^{i} \overset{t\to\infty}{=\!=} \tag{6.5}$$

$$(1-h)\left(\frac{h}{1-(1-h)}\right) = (1-h) \tag{6.6}$$

In Eq. (6.3), we write the summation from $s = 0$ to t instead of writing from $s = t$ to 0 with a negative step to avoid confusion as the end result is the same. Also, Eq. (6.5) holds as $1 - h < 1$.

We write the sum of the weights that are within the time interval $[t - w_e, t]$ equal to $p \cdot 100\%$ of the total weights as follows:

$$\sum_{\tau=t-w_e}^{t} h(1-h)^{(t-\tau)\cdot\Delta+1} = p \cdot \sum_{\tau=0}^{t} h(1-h)^{(t-\tau)\cdot\Delta+1} \tag{6.7}$$

Then, we solve in respect to h:

$$\sum_{\tau=t-w_e}^{t} h(1-h)^{(t-\tau)\cdot\Delta+1} = p \cdot \sum_{\tau=0}^{t} h(1-h)^{(t-\tau)\cdot\Delta+1} \implies \tag{6.8}$$

$$\sum_{\tau=t-w_e}^{t} h(1-h)^{(t-\tau)\cdot\Delta+1} = p(1-h) \implies \tag{6.9}$$

$$\sum_{\tau=t-w_e}^{t} h(1-h)^{(t-\tau)\cdot\Delta} = p \overset{s=\tau-t+w_e}{\implies} \tag{6.10}$$

$$\sum_{s=0}^{w_e} h(1-h)^{(w_e-s)\cdot\Delta} = p \overset{z=w_e-s}{\implies} \tag{6.11}$$

$$\sum_{z=0}^{w_e} h(1-h)^{(z)\cdot\Delta} = p \overset{i=z\cdot\Delta}{\implies} \tag{6.12}$$

$$\sum_{i=0}^{w_e/\Delta} h(1-h)^{i} = p \implies \tag{6.13}$$

$$h\frac{1-(1-h)^{w_e/\Delta+1}}{1-(1-h)} = p \implies \tag{6.14}$$

$$1-(1-h)^{w_e/\Delta+1} = p \implies \tag{6.15}$$

$$(1-h)^{w_e/\Delta+1} = 1-p \implies \tag{6.16}$$

$$(1-h) = (1-p)^{\frac{1}{w_e/\Delta+1}} \implies \tag{6.17}$$

$$h = 1-(1-p)^{\frac{1}{w_e/\Delta+1}} \tag{6.18}$$

Finally, $h = h(w_e; p, \Delta)$ is parametrized based on w_e, p and Δ as follows,

$$h(w_e; p, \Delta) \approx 1-(1-p)^{\frac{1}{w_e/\Delta+1}}. \tag{6.19}$$

For our analysis, we arbitrarily choose $p = 0.9$.

6.2 Code for EEG

6.2.1 Preprocessing Filter

```
import numpy as np
from scipy import signal

notch = 50.0
qual = 20

low_cut = 0.5
high_cat = 70

#iirnotch creates the filter and later the filtfilt
#function applies the filter to the data
b_notch, a_notch = signal.iirnotch(notch, qual, freq)

#butter_bandpass creates the filter
def butter_bandpass(lowcut, highcut, fs, order=5):
    nyq = 0.5 * fs
    low = lowcut / nyq
    high = highcut / nyq
    b, a =
        signal.butter(order,[low,high],btype='band')
    return b, a

#butter_bandpass_filter applies the filter to the data
def butter_bandpass_filter(data, lowcut, highcut,
                                    fs, order=5):
    b, a = butter_bandpass(lowcut, highcut,
                                    fs, order=order)
```

```
    y = signal.filtfilt(b, a, data)
return y

#the EEG recordings are stored in the variable data
data = np.array(...)

notch_data = signal.filtfilt(b_notch, a_notch, window_bi)

bandpass_notch_data = butter_bandpass_filter(notch_data,
                                low_cut, high_cut, freq)
```

6.2.2 Calculate the increase or decrease of variance and autocorrelation prior to a seizure event

The functions *data_to_gvar*, *data_to_exp_var* and *moving_correlation* are defined later in Appendix 6.3.

```
import numpy as np

def get_slope(data, window_size, onset, lag = -1,
                                    swift = 1, freq = 256):

    # data: onset EEG data of a seizure event
    # window_size: window length in seconds
    # onset: onset length in seconds
    # method: method to be used
    # -> g: Gaussian Weighted variance
    # -> e: Exponential Weighted Variance
```

```
# -> a: Autocorrelation
# lag: lag or autocorrelation
#          (used only if method == 'a')
# shift: swift of the window per step in time units
#          (used only if method == 'a')
# freq: sampling rate

g_var = data_to_gvar(data, window_size, d=freq)
e_var = data_to_exp_var(data, window_size, d=freq, p=0.9)
a_corr = moving_correlation(data, window_size, shift,
                lags=np.array([lag]), sample_rate=256)

# For autocorrelation the resulting timeseries have
# a sampling rate of 1/swift

a_freq = int(1/swift)



# var_times and corr_times are timeseries of the
# timesteps for each data that is resulted in each
# method
var_times = np.arange(0, len(data)//freq, 1/freq)
corr_times = np.arange(0, len(data)//a_freq, 1/a_freq)

g_params ,_ = curve_fit(lin_reg, var_times, g_var,
                method = 'lm')
e_params ,_ = curve_fit(lin_reg, var_times, e_var,
```

```
                                method = 'lm')
    a_params ,_ = curve_fit(lin_reg, corr_times, a_corr,
                                method = 'lm')

    g_sign = 1 if g_params[0] > 0 else 0
    e_sign = 1 if e_params[0] > 0 else 0
    a_sign = 1 if a_params[0] > 0 else 0

    return g_sign, e_sign, a_sign
```

6.3 Code for Feature Estimation Methods

6.3.1 Gaussian Weighted Variance

```
import numpy as np

def vnormal(arr, sd):
    vnorm = np.zeros_like(arr)

    for i in range(len(arr)):

        vnorm[i] = 1 / (sd * np.sqrt(2 * np.pi)) *
                   np.exp(-1 / 2 * (arr[i] / sd) ** 2)

    return vnorm

def gausian_variance(data, d=20):
```

```
    window = int(len(data) / d)

    gstd = window / 6

    half = window / 2

    weights = vnormal(np.arange(-half, half, 1 / d),
                                                gstd)


    gvar = weights.sum() / (weights.sum() ** 2 -
                (weights ** 2).sum()) *
                ((weights * (data ** 2))).sum()


    return gvar

def data_to_gvar(sss, interval, d=20, detrended=False):
    window = int(interval * d)

    assert window < len(sss)

    var_list = np.zeros_like(sss[window:])
    assert len(var_list) == len(range(window, len(sss)))

    for i in range(window, len(sss)):
```

```
            var_list[i - window] =
                        gausian_variance(sss[i - window:i],
                                         d=d, detrended=detrended)

    return var_list
```

6.3.2 Exponential Weighted Variance

```
import numpy as np
def data_to_exp_var(sss, interv, d=256, p=0.9):
    h = (1 - (1 - p) ** (1 / interv / d))

    mmean = np.zeros_like(sss)
    vvar = np.zeros_like(sss)

    mmean[0] = np.mean(sss[0:interv * d])
    vvar[0] = np.var(sss[0:interv * d])

    for i in np.arange(1, len(sss)):
        vvar[i] = (1 - h) * (vvar[i - 1] + h *
                                    (sss[i]) ** 2)

    return vvar
```

6.3.3 Autocorrelation

```
import numpy as np
```

```
def correlation_func(x, y):
    if x.size != y.size:
        print('Not correct size for x and y ')
        return None

    sdx = np.std(x)
    sdy = np.std(y)

    if sdx == 0 or sdy == 0:
        print(sdx)
        print(sdy)

        print('Standerd deviation equal zero')

        return 0
    n = x.size

    x2 = x * x
    y2 = y * y
    xy = x * y

    cor = np.sum(xy) / (np.sqrt(np.sum(x2)) *
                                np.sqrt(np.sum(y2)))

    return cor
```

```
def auto_correlation(x, lag=1):
    if len(x) == 0 or len(x) == 1:

        return 0

    elif len(x) == 2:
        return 1

    sdx = np.std(x[lag:])
    #
    sdy = np.std(x[:len(x) - 1 - lag])

    # return 0
    if ((sdx == 0) or (sdy == 0)):
        print(sdx)
        print(sdy)

        print('Standerd deviation equal zero')

        return 0

    if lag == 0:

        return 1

    elif ((lag > 0) and (lag < len(x))):
```

```
        return correlation_func(x[lag:], x[:-lag])

    else:
        print('Not valid lag')
        return 0

def moving_correlation(data, interv, shift,
                lags=np.array([1]), sample_rate=256):



return_list = np.zeros((len(lags), len(range(int(interv *
                    sample_rate), len(data), int(shift *
                    sample_rate)))),dtype=np.float64)


for en,lag in np.ndenumerate(lags):

    corr = np.zeros_like(np.arange(int(interv *
                        sample_rate), len(data),
                        int(shift * sample_rate)),
                        dtype=np.float64)

    assert len(corr) == len(range(int(interv *
                        sample_rate), len(data),
                        int(shift * sample_rate)))
```

```
    for i in np.arange(0, len(corr)):
        temp = auto_correlation(
            data[int(i * shift * sample_rate):int(i *
                    shift * 6sample_rate + interv *
                    sample_rate)], lag=lag)

        corr[i] = temp

    return_list[en][0:len(corr)] = corr

return return_list
```

6.4 Code for Harvested Population system

6.4.1 Bifurcation Diagram

```
from sympy import *

# Defining the symbols used
# x: the state of the system
# c: bifurcation parameter
# k: carrying capacity sset to 10
x, c, k = symbols('x c k')

# Defining the equation
f =x*(1-x/k)-c*x*x/(x*x+1)
```

```
# Getting the first derivative for later use
fx = diff(f,x)

# Getting the integral for later use
# We calculate each part separately for efficiency
U = -integrate(x*(1-x/k),x)-integrate(-m*x*x/(x*x+1),x)

# Getting the potential derivative

Ux = diff(U,x)

# Getting the potential second derivative

Uxx = diff(Ux,x)

# Getting the solutions for x'=0
solutions = solve(f,x)

# Solutions is a list of 4 elements.
# Each element is the function of each branch of
# equilibria of the bifurcation diagram
# as shown in Figure 3.1
```

6.4.2 Numerical calculations of the Harvested population and the linearized Harvested population system

```
import numpy as np

# hp_sys returns the next value of the HP system
def hp_sys(x, c, dt=0.01, D=0.2):

    new_x = x + dt*(x*(1-x/10)-c*x**2/(x**2+1))
                +np.sqrt(D*dt)*np.random.normal()

    # if new_x < 0, we return 0 as the HP system
    # is not defined for negative values
    # the equations still hold but the model it
    # represents does not allow negative values
    if new_x >=0:
        return new_x
    else:
        return 0

# lin_sys returns the next value of the linearized
# HP system
def lin_sys(x,l,x_0,dt = 0.01,D=0.2):

    return x-dt*l *(x-x_0)
                  +np.sqrt(dt*D)*np.random.normal()

import numpy as np

def HP(c, N, cr = 0, dt = 0.01, D = 0.2):
```

```
# c: Initial values for the bifurcation parameter
# N: number of steps performed
# dt: timestep
# D: noise strength

# xlist is the values of the resulting time-series
# of the HP system
xlist = np.zeros(N,dtype = np.float64)

# As the solutions for the equilibria is too
# complex to provide in analytical formulas
# we initialize at x=10 and let the system
# evolve for 10000 steps without noise (D = 0)
# to find the equilibrium
init_N = 10000
temp_xlist = np.zeros(init_N, dtype = np.float64)
temp_xlist[0] = 10
for i in np.arange(1,init_N):
    temp_xlist[i] = hp_sys(temp_xlist[i-1],
                           c, dt = dt,D = 0)

# Inisiatize the system at the equiolibrium
xlist[0] = temp[-1]

for i in np.arange(1,N):

    if cr != 0:
```

```
            c += cr

        xlist[i] = hp_sys(xlist[i-1],c, dt = dt, D = D)

    return xlist[:]

def dyn_HP(time, c_0, c_f, dt = 0.01, D = 0.2):
    # time: time in time units for the simulation
    # c0: inital value for c
    # cf: final value for c
    # dt: timestep
    # D: noise

    # N: time of steps performed
    N = time / dt

    if N % 1 !=0:
        print("Steps were missed")

    N = int(N)

    # cr: cr: rate of change of c per step
    cr = (c_f - c_0)/N

    xlist = HP(c_0, N,cr = cr, dt = dt, D = 0.2)
    return xlist[:]
```

Bibliography

[1] Geraldine B. Boylan, Liudmila Kharoshankaya, and Sean R. Mathieson. Chapter 18 - diagnosis of seizures and encephalopathy using conventional EEG and amplitude integrated EEG. In *Neonatal Neurology*, volume 162 of *Handbook of Clinical Neurology*. Elsevier, 2019.

[2] Martha Buckley and John Marshall. Observations, inferences, and mechanisms of the atlantic meridional overturning circulation: A review. *Reviews of Geophysics*, 2015.

[3] R.R. Clancy and A. Legido. The exact ictal and interictal duration of electroencephalographic neonatal seizures. *Epilepsia*, 28(5), 1987.

[4] Westinghouse Electric Corporation. *Electrical transmission and distribution reference book*. Westinghouse electric corporation, 1964.

[5] Lorenzo Fabrizi, Madeleine Verriotis, Gemma Williams, Amy Lee, Judith Meek, Sofia Olhede, and Maria Fitzgerald. MRI findings in infants with infantile spasms after neonatal hypoxic-ischemic encephalopathy. *Scientific Reports*, 49(6), 2013.

[6] Dean R. Freestone, Philippa J. Karoly, Andre D. H. Peterson, Levin Kuhlmann, Alan Lai, Farhad Goodarzy, and Mark J. Cook. Seizure pre-

diction: Science fiction or soon to become reality? *Curr Neurol Neurosci Rep*, 15, 2015.

[7] Crispin Gardiner. *Stochastic methods, A Handbook for the Natural and Social Sciences*. Springer, 2009.

[8] Viktor Jirsa, William Stacey, Pascale Quilichini, Anton Ivanov, and Christophe Bernard. On the nature of seizure dynamics. *Brain : A journal of neurology*, 137, 2014.

[9] Allen A. Kimberly and Brandon H. Debra. Hypoxic ischemix encephalopathy: Pathophysiology and experimental treatments. *Newborn and Infant Nursing reviews*, 11, 2011.

[10] Christian Kuehn. A mathematical framework for critical transitions: Bifurcations, fast–slow systems and stochastic dynamics. *Physica D: Nonlinear Phenomena*, 240(12):1020–1035, 2011.

[11] Cian McCafferty, Benjamin F. Gruenbaum, and Renee Tung. Decreased but diverse activity of cortical and thalamic neurons in consciousness-impairing rodent absence seizures. *Nature Communications*, 14(1), 2023.

[12] Piotr Milanowski and Piotr Suffczynski. Seizures start without common signatures of critical transition. *International journal of neural systems*, 26:1650053, 2016.

[13] Abraham Peliowski-Davidovich, Canadian Paediatric Society, Fetus, and Newborn Committee. Hypothermia for newborns with hypoxic ischemic encephalopathy. *Paediatrics & child health*, 17(1):41–43, 2012.

[14] Georgia Ramantani, Bernhard Schmitt, Barbara Plecko, Ronit Pressler, Gabriele Wohlrab, Katrin Klebermaß-Schrehof, Cornelia Hagmann,

Francesco Pisani, and Geraldine Boylan. Neonatal seizures—are we there yet? *Neuropediatrics*, 50, 2019.

[15] Harvey B. Sarnat and Margaret S. Sarnat. Neonatal Encephalopathy Following Fetal Distress: A Clinical and Electroencephalographic Study. *Archives of Neurology*, 33(10), 1976.

[16] Marten Scheffer, Jordi Bascompte, William Brock, Victor Brovkin, Stephen Carpenter, Vasilis Dakos, Hermann Held, Egbert Nes, and Max Rietkerk. Early-warning signals for critical transitions. *Nature*, 461, 2009.

[17] Marten Scheffer, Steve Carpenter, Jonathan A Foley, Carl Folke, and Brian Walker. Catastrophic shifts in ecosystems. *Nature*, 413(6856):591–596, 2001.

[18] Gyu Hong Shim. Which factors predict outcomes of neonates with hypoxic-ischemic encephalopathy following therapeutic hypothermia? *Clinical and Experimental Pediatrics*, 64, 2020.

[19] Saurabh Sinha, Lucy Sullivan, Dragos Sabau, and Daniel San-Juan *et al.* American Clinical Neurophysiology Society Guideline 1: Minimum Technical Requirements for Performing Clinical Electroencephalography. *Journal of clinical neurophysiology*, 33(4), 2016.

[20] Steven Strogatz. *Nonlinear dynamics and chaos : with applications to physics, biology, chemistry, and engineering.* Cambridge, 2001.

[21] A Temko, E Thomas, W Marnane, G Lightbody, and G Boylan. EEG-based neonatal seizure detection with support vector machines. *Clinical neurophysiology*, 122, 2011.

[22] Eric Zivot and Jiahui Wang. *Modeling financial time series with S-PLUS*, volume 2. Springer, 2006.